

# **Final Report**

Numerical Investigation into the Significance of Night Time Evaporation from Irrigation Farm Dams Across Australia

> Matthew R. Hipsey Centre for Water Research, University of Western Australia

> > September 2006

# Disclaimer

The information contained in this publication is intended for general use, to assist public knowledge and discussion, and to help improve the sustainable management of land, water and vegetation. It includes general statements based on scientific research. Readers are advised and need to be aware that this information may be incomplete or unsuitable for use in specific situations. Before taking any action or decision based on the information in this publication, readers should seek expert professional, scientific and technical advice.

To the extent permitted by law, the Commonwealth of Australia, Land & Water Australia (including its employees and consultants), the authors, the Centre for Water Research, University of Western Australia and the National Program for Sustainable Irrigation and its partners do not assume liability of any kind whatsoever resulting from a person's use or reliance upon the content of this publication.

The National Program for Sustainable Irrigation focuses research on the development and adoption of sustainable irrigation practices in Australian agriculture. The aim is to address critical emerging environmental management issues while generating long-term economic and social benefits that ensure irrigation has a viable future. The Program has fourteen funding partners who are: Land & Water Australia (Managing Partner); Department of Agriculture, Fisheries and Forestry; Department of Natural Resources and Mines, Queensland; Department of Primary Industries & Resources, South Australia; Department of Environment Water & Catchment, Western Australia; Department of Agriculture, Western Australia; Cotton Research & Development Corporation; Horticulture Australia; Goulburn-Murray Water, Victoria; Harvey Water, Western Australia; Lower Murray Water Authority, Victoria; Sunwater, Queensland; Grampians Wimmera Mallee Water, Victoria and the Ord Irrigation Cooperative, Western Australia.

#### © Land & Water Australia, 2006

Material from this publication may not be used unless prior written approval has been obtained from the National Program for Sustainable Irrigation.

Published by: Land & Water Australia on behalf of

the National Program for Sustainable Irrigation

Postal address: GPO Box 2182

Canberra ACT 2601

Office Location: L1. The Phoenix Building

86 Northbourne Ave

**Braddon ACT** 

Telephone: 02 6263 6000

Internet: www.npsi.gov.au

Product Code: ER061199 ISBN: 1 921253 16 9

# **EXECUTIVE SUMMARY**

This report documents the numerical analysis performed for the Land and Water Australia (LWA) National Program for Sustainable Irrigation project "The significance of night time evaporation from irrigation farm dams" under contract UWA45. The objective of the present study is to further develop the numerical model DYRESM to make it applicable to irrigation farm dams and to subsequently apply it to gain insights into night time evaporation.

Evaporation is a significant loss component from irrigation dams, and although numerous evaporation reduction methodologies exist, their adoption is hindered since they are deemed uneconomical. Any cost/benefit analyses that are done are generally based on poor evaporation estimates due to the complexities involved in evaporation prediction. One area of uncertainty is the significance of night time evaporation. Similarly, the role of windsheltering on evaporation can be significant but is rarely accounted for in any quantitative assessment. There is therefore a need for improved estimates of evaporation so that water management and investment decisions can have a quantitative basis. Specifically, it has been the aim of this project to ascertain the importance of night time evaporation and to provide quantitative estimates of its significance across a range of climatic regions. An additional objective was to compare the current methodology with that presented herein.

For this analysis the hydrodynamic model DYRESM was used to simulate 10 idealised dams ranging in geographic location and morphometry. DYRESM was used to simulate the water balance and thermal structure of the dams, and in particular estimate the evaporative fluxes. The evaporative flux measurements were corrected for non-neutral atmospheric conditions, still-air conditions and for the effect of wind-sheltering.

Irrespective of a dam's size or the climatic region it is located in, the contribution of evaporation during the night was found to be considerable. Predictions from the 10 test dams suggest that between 35 - 45% of the total annual loss of water through evaporation occurred during the night. In a climate where potential evaporation is approximately 1.5 m year<sup>-1</sup>, this equates to roughly 0.6 m year<sup>-1</sup>. It was observed that most of the variability seen in the night time evaporation fraction was due to climate.

Although the magnitude of the variation differed between regions, all simulations showed significant seasonal variability in the night time fraction of evaporation. In particular, it was predicted that the night time contribution increased considerably during the winter months, with all sites showing the fraction increasing to 55 – 70%. This increase correlated well with an increase in the number of low wind hours and local instability over the water surface suggesting an increase in the frequency of free convective losses is responsible. Overall however, the analysis concluded that the fraction of evaporation occurring during the night time is largely insensitive to climate or dam morphometry. Evaporation mitigation strategies should therefore target the driving mechanisms causing the evaporative flux by reducing wind speed, and limiting solar heating.

Finally, it was found that using DYRESM without the advanced flux corrections still captured the dominant behaviors and could safely be used over suitably long time integrations for routine water balance assessments. However, the use of the simple flux calculation with poor surface water temperature data or predictions is problematic.

As part of this project, DYRESM (with the improvements implemented during this analysis) is to be made available freely online to aid engineers and water managers design efficient irrigation storages. The advantages of using a common framework for routine water balance assessments are also discussed.

# **CONTENTS**

1	INTRODUCTION	5
	1.1 Background	5
	1.2 Aims & Objectives	
2	METHODOLOGY	6
	2.1 General Approach	6
	2.2 MODEL DESCRIPTION	7
	2.2.1 DYRESM	
	2.2.2 Surface thermodynamics model	
	2.2.2.1 Non-neutral atmospheric stability	
	2.2.2.2 Still-air limit	
	2.2.2.3 Wind-sheltering	
	2.3 MODEL APPLICATION	
	2.3.1 Test sites	
	2.3.2 Morphometry	
	2.3.3 Meteorological forcing	
	2.4 CONFIGURATION DETAILS	
3		
•	3.1 SIMULATION RESULTS	
	3.1.1 Water column stratification	
	3.1.2 Atmospheric instability	
	3.1.3 Evaporative flux rates	
	3.2 EVAPORATION ANALYSIS	
	3.3 MODEL COMPARISON WITH EXISTING METHODOLOGY	39
4	DISCUSSION & CONCLUSIONS	41
	4.1 Role of night time evaporation	41
	4.2 IMPLICATIONS FOR RESERVOIR DESIGN AND MANAGEMENT AND EVAPORATION	
	AMELIORATION	42
5	REFERENCES	44



## 1 Introduction

# 1.1 Background

This report documents the numerical analysis performed for the Land and Water Australia (LWA) National Program for Sustainable Irrigation project "The significance of night time evaporation from irrigation farm dams" under contract **UWA45**. The objective of the present study is to further develop the numerical model DYRESM to make it applicable to irrigation farm dams and to subsequently apply it to gain insights into night time evaporation.

The National Program for Sustainable Irrigation (NPSI) has highlighted the importance of understanding evaporation from dams and has recently undertaken a scoping study on evaporation reduction methodologies (Watts, 2005). A range of evaporation reduction methodologies exist, but often their adoption is hindered since they are deemed uneconomical. Any cost/benefit analyses that are done are generally based on poor evaporation estimates due to the complexities involved in evaporation prediction. For example, there is a common misconception that evaporation at night time is negligible although it has been observed to be appreciable in farm dams in Western Australia due to local atmospheric instability near the surface (Hipsey et al. 2004). Similarly, the role of wind-sheltering on evaporation can be significant (Hipsey et al., 2003; Condie and Webster, 1995), but unfortunately these factors are rarely accounted for in any quantitative assessment. There is therefore a need for improved estimates for evaporation so that water management and investment decisions can have a quantitative basis.

# 1.2 Aims & Objectives

The objectives of this report are to:

- 1. To ascertain the importance of night time evaporation from farm dams across a range of climatic zones.
- 2. To quantify the day-time vs. night time losses in the different climatic zones and for different seasons.
- 3. To examine the sensitivity of evaporation predictions to humidity, temperature and atmospheric stability, dam morphometry, wind, and wind-sheltering.
- 4. To assess the robustness of the current evaporation prediction framework outlined in the scoping study, and provide an improved framework for engineers to estimate evaporation given routine meteorological and morphological information.

## 2 METHODOLOGY

# 2.1 General Approach

There are three important considerations in a quantitative analysis of evaporation from irrigation farm dams. First, to resolve sub-daily evaporation variability (i.e., day time vs. night time evaporation fluxes) it is insufficient to apply the commonly used 'bulk-transfer' evaporation equation with a constant evaporation coefficient as is usually done. This methodology assumes a neutrally buoyant atmospheric boundary layer above the water, which is only a safe assumption for daily or longer time integrations. In reality of course, the surface water temperature of the dam varies much less over a day than the air temperature, and so stable and unstable boundary layers will evolve over the course of the day. This variability greatly impacts evaporation (Condie and Webster, 1997; Hipsey et al., 2004) and needs to be accounted for in any quantitative assessment. Second, evaporation dynamically affects water temperature and this is an important feed back to consider when predicting evaporative losses. Diurnal water temperature variability will also play an important role in driving night time vs. day time fluxes. Third, under low wind conditions that are typical during the summer months, convectively driven atmospheric motions drive the evaporative flux, and this can form a substantial component of the daily evaporation volume.

Given these three considerations, the model DYRESM was selected for use in this investigation. DYRESM is designed for long-term simulations of lake and reservoir hydrodynamics, and in particular for capturing vertical temperature stratification. It also accounts for sub-daily meteorological variability (including the effects of clouds, humidity, air temperature, wind and solar radiation) and importantly, includes corrections for non-neutral atmospheric stabilities. DYRESM is an easy to use, freely-distributed model developed by CWR that is currently used in over 80 countries with approximately 1500 registered users. For the purposes of this study, we also include a correction for wind-sheltering into the DYRESM evaporation algorithms based on that presented by Hipsey *et al.* (2003), and a low-wind evaporation equation designed for when convectively driven process dominate. These are of particular importance to farm dams, as these authors have shown that evaporation can still occur when there is no wind and no solar radiation input. The model is described in detail in Section 2.2 below.

To test the sensitivity of the model to various dam morphometries and climates, a range of test sites were identified typical of those found across Australia. The sites chosen were based on land-use relevance and meteorological data availability. For each site, three different size dam morphometries were developed to shed light on the sensitivity of

evaporation to surface-area volume relationship. The sizes chosen are based on the sizes typical of the particular climatic zone. An overview of the test sites is outlined in Section 2.3.

For each simulation, an analysis was performed to ascertain the role of night time vs. day time evaporation, and the causal factors creating the predicted response. To understand the differences between the framework presented here and the currently accepted framework (as outline in Watts, 2005), the simulations were then rerun with wind-sheltering and no correction for non-neutral atmospheric stabilities.

# 2.2 Model Description

## **2.2.1 DYRESM**

DYRESM (**DY**namic **RES**ervoir **S**imulation **M**odel) is a one-dimensional hydrodynamics model for predicting the vertical distribution of temperature, salinity and density in lakes. The model is based on an assumption of one dimensionality; that is, the variations in the vertical play a more important role than those in the horizontal direction. This gives rise to the layer construction, in which the reservoir is represented as a series of horizontal layers. There is no lateral or longitudinal variation in the layers, and the vertical profile in any property is obtained from the property values from each layer.

The one-dimensional approximation is valid when the forces acting to destabilize a water body (wind stress, surface cooling or plunging inflows) do not act over prolonged periods of time. The dynamics of many lakes and reservoirs, viewed over time scales longer than those of extreme events such as storms and floods, are well described using this approximation. DYRESM provides quantifiably verifiable predictions of the thermal characteristics in such systems over time scales ranging from several weeks to tens of years. The model thus provides a means of predicting seasonal and inter-annual variability of lakes and reservoirs as well as sensitivity testing to long-term changes in environmental factors or watershed properties.

Since DYRESM runs at a sub-daily time step (e.g. hourly), it should be noted that during a wind event warmer water will tend to accumulate at the downwind end of the lake, thereby creating alongwind gradients in both the surface water temperature and also in the atmospheric vapour pressure. It is not possible to resolve these gradients in a 1D model, and since the wind field is varying in direction, a full 3D model of both the waterbody and the atmospheric boundary layer would be required. Such an analysis is beyond the present scope of work since it would be difficult to extend to year long simulations due to problems with numerical diffusion and computational demand. Fortunately, Condie and Webster (1997)

performed a detailed analysis on these alongwind gradients using a 2D coupled waterbody-boundary layer model and concluded that the increased in downwind surface temperature is roughly offset by the increased atmospheric vapour pressure. That is, the alongwind gradients created no significant net effect on the evaporative or sensible heat flux.

DYRESM parameterizes the important physical processes leading to temporal changes in the temperature, salinity and density distributions in lakes and reservoirs. The model relies on parameterisations derived from detailed process studies (both from the field and in the laboratory). Although DYRESM is considered a 1D model, it parameterises 3D processes such as inflows and boundary mixing. Additionally, DYRESM is unique since it is based on a Lagrangian (moving) grid and thus doesn't suffer from the problems of numerical diffusion that affect fixed-grid models run over long periods.

DYRESM operates based on the principles of conservation of mass, momentum and heat. Mass is modelled by considering inflows, outflows, evaporation and rainfall. Momentum is modelled based on wind input, inflow input and drag. The surface thermodynamics module is described separately in detail below. The various parameters required by DYRESM are largely physically-based and require little or no adjustment by the user.

Since DYRESM is laterally averaged, there is no need for detailed bathymetry to be provided; instead the model simply requires a stage-area relationship (i.e. depth vs. surface area). Forcing data required includes surface meteorological data (solar radiation, longwave radiation/cloud cover, wind speed, air temperature and relative humidity) and inflow/outflow properties (volume, temperature and salinity). An overview of the files needed and simulation procedure is shown in Figure 1.

#### 2.2.2 Surface thermodynamics model

The surface heat, mass and momentum exchange comprise the primary driving mechanisms for DYRESM. It is these surface exchanges that provide the majority of the energy for heating, mixing and stratifying the lake. The surface exchanges include heating due to short wave radiation penetration into the lake and the fluxes at the surface due to evaporation, sensible heat (i.e. convection of heat from the water surface to the atmosphere), long wave radiation and wind stress (Figure 2). Since the primary interest here is evaporation, the remainder of this section details the bulk flux calculations; for other detail on other aspects the reader is directed to the DYRESM science manual available from http://www.cwr.uwa.edu.au/.

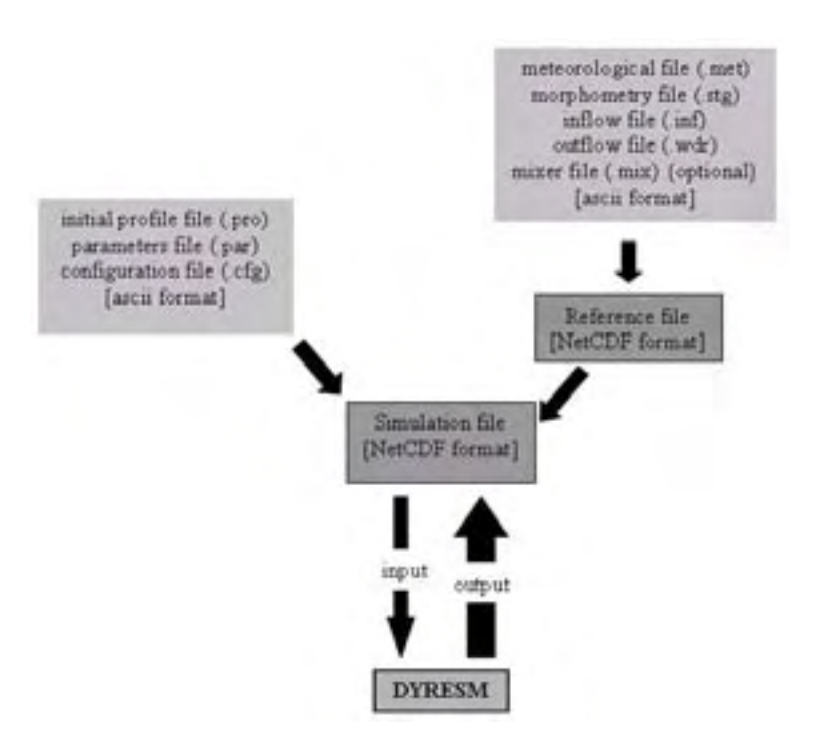


Figure 1: Outline of the data and files required for a DYRESM simulation, and schematic representation of a typical simulation sequence.

For calculation of the fluxes of momentum and sensible and latent heat from the water surface to the atmosphere DYRESM employs the familiar bulk aerodynamic formulae, which have been shown to competently capture the surface fluxes of momentum, and sensible and latent heat from a variety of water bodies:

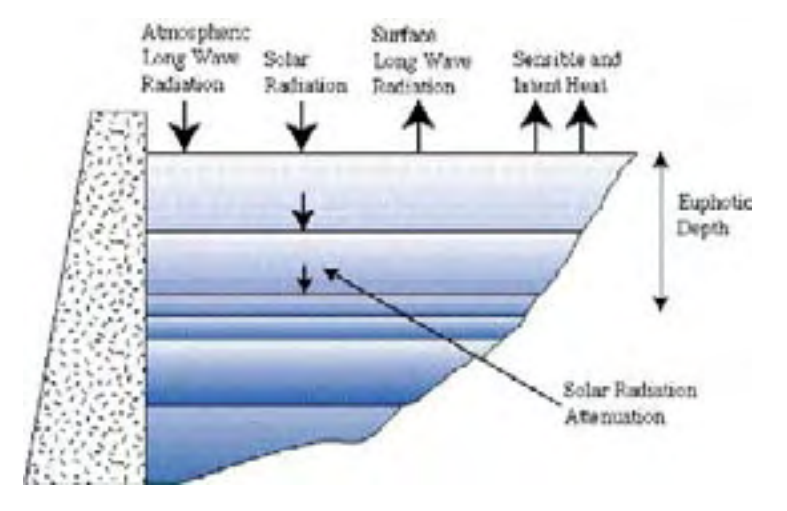


Figure 2: Surface thermodynamics processes simulated by DYRESM.

$$\tau = \rho \overline{u'w'} = \rho C_D U_z^2 \tag{1}$$

$$H = \rho c_p \overline{\theta' w'} = -\rho c_p C_H U_z (\theta_z - \theta_s)$$
 (2)

$$E = \rho \lambda \overline{q'w'} = -\rho \lambda C_F U_z (q_z - q_s)$$
(3)

where  $\tau$  is the surface stress, H is sensible heat, E is latent heat.  $\rho$  is air density,  $c_{\rho}$  is the specific heat of air,  $\lambda$  is the latent heat of vaporization, u' and w' are the turbulent velocity fluctuations in the horizontal and vertical directions respectively, and the overbar indicates a time average.  $U_z$ ,  $\theta_z$  and  $q_z$  are the wind speed, temperature and humidity respectively at height z above the water, and  $\theta_s$  and  $q_s$  are the temperature and humidity values at the water surface.

Longwave can either be supplied directly, or should no data exist, DYRESM can calculate the longwave budget from cloud cover (as is done in this study). The longwave radiation energy density incident on the water surface is estimated as:

$$Q_{LW_{(NT)}} = (1 - r_{lw})Q_{LW_{(N)}} - Q_{LW_{(OUT)}}$$
(4)

where  $r_{lw}$  is the surface albedo for longwave radiation. The incoming longwave is an empirical function of the cloud cover fraction, C, as given by:

$$Q_{LW_{(IN)}} = (1 + 0.17C^2)\varepsilon_a(\theta_a)\sigma\theta_a^4$$
(5)

where the emmisivity of the atmosphere is modelled according to Swinbank (1963):

$$\varepsilon_a(\theta_a) = c_e \theta_a^2 \tag{6}$$

with  $c_e = 9.37 \times 10^{-6} \text{ K}^{-2}$ . Long wave radiation emitted from the water surface is given by Stefan-Boltzmann equation:

$$Q_{LW_{(OUT)}} = \varepsilon_{w} \sigma \theta_{w}^{4} \tag{7}$$

where  $\varepsilon_{w}$  is the emissivity of the water surface (=0.96),  $\sigma$  is the Stefan-Boltzmann constant  $(\sigma = 5.6697 \times 10^{-8} \text{ W m}^{-2} \text{ K}^{-4}).$ 

#### 2.2.2.1 Non-neutral atmospheric stability

For long time integrations (i.e. seasonal), the bulk-transfer coefficients for momentum,  $C_D$ , sensible heat,  $C_H$ , and latent heat,  $C_E$ , can be assumed approximately constant because of the negative feedback between surface forcing and the water body's temperature response (e.g. Strub and Powell, 1987). At finer timescales (hours to weeks), the thermal inertia of the water body is too great and so the transfer coefficients must be specified as a function of the degree of atmospheric stratification experienced in the internal boundary layer that develops over the water. Monin and Obukhov (1954) parameterised the stratification seen in the air column using the now well-known stability parameter, z/L, where L is the Obukhov length defined as:

$$L = \frac{-\rho u_*^3 \theta_v}{kg \left[ \frac{H}{c_p} + 0.61 \frac{\theta E}{\lambda} \right]}$$
 (8)

Here, k is the von Karman constant,  $u_*$  is the friction velocity and  $\theta_v = \theta(1 + 0.61q)$  is the virtual temperature. Paulson (1970) presented a solution for the vertical profiles of wind speed, temperature and moisture in the developing boundary layer as a function of the Monin-Obukhov stability parameter; the so-called flux-profile relationships:

$$U = \frac{u_*}{k} \left[ \ln \left( \frac{z}{z_o} \right) - \psi_M \left( \frac{z}{L} \right) \right] \tag{9}$$

$$\theta_z - \theta_s = \frac{\theta_*}{k} \left[ \ln \left( \frac{z}{z_\theta} \right) - \psi_H \left( \frac{z}{L} \right) \right] \tag{10}$$

$$q_z - q_s = \frac{q_*}{k} \left[ \ln \left( \frac{z}{z_q} \right) - \psi_E \left( \frac{z}{L} \right) \right]$$
 (11)

where  $\psi_M$ ,  $\psi_H$  and  $\psi_E$  are the similarity functions for momentum, heat and moisture respectively, and  $z_0$ ,  $z_\theta$  and  $z_q$  are their respective roughness lengths. For unstable conditions (L<0), the stability functions are defined as (Paulson 1970; Businger et al., 1971; Dyer, 1974):

$$\psi_M = 2\ln\left(\frac{1+x}{2}\right) + \ln\left(\frac{1+x^2}{2}\right) - 2\tan^{-1}(x) + \frac{\pi}{2}$$
 (12)

$$\psi_H = \psi_E = 2\ln\left(\frac{1+x^2}{2}\right) \tag{13}$$

where

$$x = \left[1 - 16\left(\frac{z}{L}\right)\right]^{1/4}$$

During stable stratification (L>0) they take the form:

$$\psi_{M} = \psi_{H} = \psi_{E} = \begin{cases} -5\left(\frac{z}{L}\right) & 0 < \frac{z}{L} < 0.5 \\ 0.5\left(\frac{z}{L}\right)^{-2} - 4.25\left(\frac{z}{L}\right)^{-1} - 7\ln\left(\frac{z}{L}\right) - 0.852 & 0.5 < \frac{z}{L} < 10.0 \\ \ln\left(\frac{z}{L}\right) - 0.76\left(\frac{z}{L}\right) - 12.093 & \frac{z}{L} > 10.0 \end{cases}$$
(14)

Substituting equations (1)-(3) into (9)-(11) and ignoring the similarity functions leaves us with neutral transfer coefficients as a function of the roughness lengths:

$$C_{XN} = k^2 \left[ \ln \left( \frac{z}{z_o} \right) \right]^{-1} \left[ \ln \left( \frac{z}{z_X} \right) \right]^{-1}$$
 (15)

where N denotes the neutral value and X signifies either D, H or E for the transfer coefficient and o,  $\theta$  or q for the roughness length scale. Inclusion of the stability functions into the substitution and some manipulation (Imberger and Patterson, 1990; Launianen and Vihma, 1990) yields the transfer coefficients relative to these neutral values:

$$\frac{C_X}{C_{XN}} = \left[ 1 + \frac{C_{XN}}{k^2} \left( \psi_M \psi_X - \frac{k \psi_X}{\sqrt{C_{DN}}} - \frac{k \psi_M \sqrt{C_{DN}}}{C_{XN}} \right) \right]$$
 (16)

Hicks (1975) and Launianen and Vihma (1990) suggested an iterative procedure to solve for the stability corrected transfer coefficient using (16) based on some initial estimate of the neutral value. The surface flux is subsequently estimated according to (1-3) and used to provide an initial estimate for L (equation 8). The partially corrected transfer coefficient is then recalculated and so the cycle goes. Strub and Powell (1987) and Launiainen (1995), presented an alternative based on estimation of the bulk Richardson number, Ri<sub>B</sub>, defined as:

$$Ri_{B} = \frac{gz}{\theta_{v}} \left( \frac{\Delta\theta + 0.61\theta_{v}\Delta q}{U^{2}} \right) \tag{17}$$

and related as a function of the stability parameter, z/L, according to:

$$Ri_{B} = \frac{z}{L} \left( \frac{k\sqrt{C_{DN}}/C_{HWN} - \psi_{HW}}{\left(k/\sqrt{C_{DN}} - \psi_{M}\right)^{2}} \right)$$
(18)

where it is specified that  $C_{HN} = C_{WN} = C_{HWN}$ . Figure 3 illustrates the relationship between the degree of atmospheric stratification (as described by both the bulk Richardson number and the Monin-Obukhov stability parameter) and the transfer coefficients scaled by their neutral value.

The iterative procedure used in this analysis is conceptually similar to the methodology discussed in detail in Launiainen and Vihma (1990). The first estimate for the neutral drag coefficient is specified as a function of windspeed (and hence the momentum roughness length) as it is has been commonly observed that  $C_{DN}$  increases with  $U_{10}$ . This is modelled according to:

$$C_{DN-10} = \begin{cases} 1.00 \times 10^{-3} & U_{10} < 5.0 ms^{-1} \\ (1.00 + 0.07[U_{10} - 5.00]) \times 10^{-3} & U_{10} \ge 5.0 ms^{-1} \end{cases}$$
(19)

which is empirically based on data from Hicks (1972), Francey and Garratt (1978) and Hicks (1975). The neutral humidity/temperature coefficient,  $C_{HWN-10}$ , is held constant at  $1.25 \times 10^{-3}$  $(1.9 \times 10^{-3})$  at z = 2.0 m). This is somewhat of a restrictive assumption as it inherently assumes the temperature and humidity roughness lengths are invariant with wind speed and therefore state of the surface waves.

#### 2.2.2.2 Still-air limit

The above analysis only applies so long as sufficient wind exists and creates a defined boundary layer over the surface of the water. As the wind tends to zero (the 'still-air limit') equations (1-3) are no longer appropriate as they do not account for free-convection directly from the water surface. This is a relatively important phenomenon for small dams since they tend have small fetches for wind speeds to build up, they have surface temperatures warmer than the atmosphere for considerable periods, and they are often sheltered from the wind.

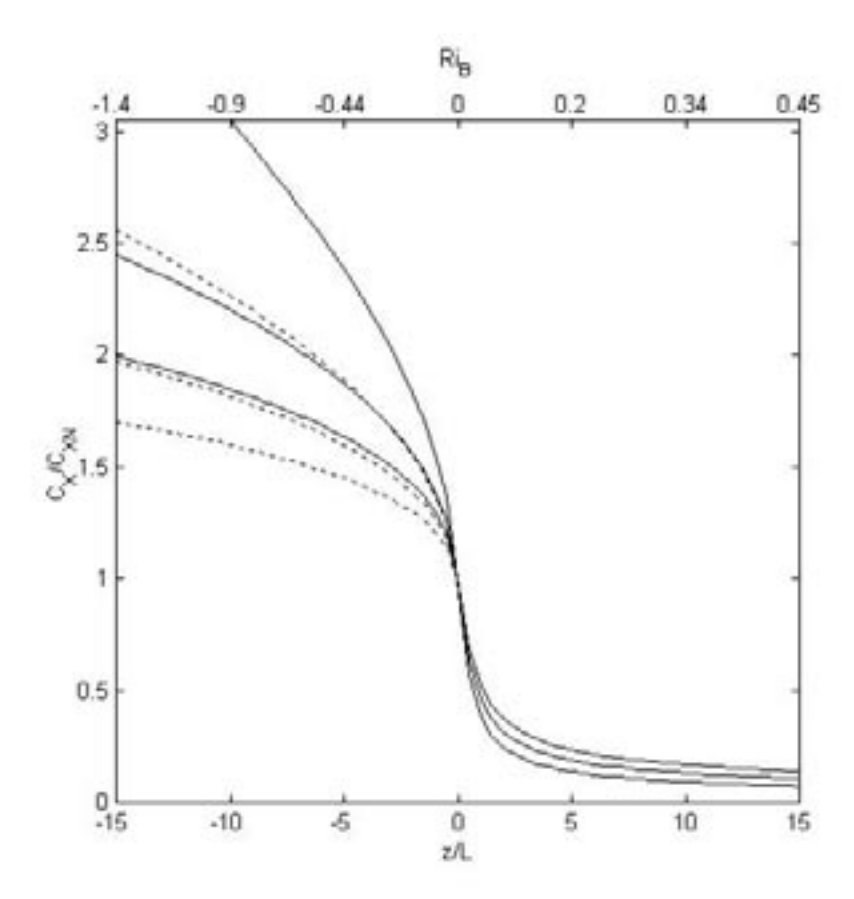


Figure 3: Relationship between atmospheric stability (bottom axis -z/L, top axis  $-Ri_B$ ) and the bulk-transfer coefficients relative to their neutral value ( $C_X/C_{XN}$  where X represents D, H or W) for several roughness values. The solid line indicates the momentum coefficient variation ( $C_D/C_{DN}$ ) and the broken line indicates humidity and temperature coefficient ( $C_{HW}/C_{HWN}$ ) variation.

For this work the atmosphere-surface heat flux algorithms of DYRESM were augmented by additional calculations to ensure that low wind-speed results were better modelled. The flux estimates are modified in DYRESM by calculating the evaporative and sensible heat flux values for  $U_{wind} = 0$  and the given  $U_{wind}$  and taking the maximum magnitude of this pair as the result; *i.e.*,

$$|Q| = max (|Q_{zero wind}|, |Q_{wind}|)$$
 (20)

for both evaporative and sensible heat fluxes.  $Q_{wind}$  is calculated from the equations of outlined above and  $Q_{zero\ wind}$  calculations are given below. The two zero-wind speed heat flux equations are taken from (TVA, 1972). These equations have been modified slightly in the program to return power flux densities in SI units (*i.e.*, W m<sup>-2</sup>). The zero wind speed evaporative heat flux calculation is described as:

$$\alpha_e = 0.137 \, \xi \, v / (c_p \, \rho_{surf}) \, [g \, (\rho_a - \rho_o) \, / \, (\rho_a \, v \, a)]^{1/3}$$
 (21a)

$$E = \alpha_e (C_o - C_a), \tag{21b}$$

where  $C = \mathcal{E} e/p$  (with the appropriate e to get C for both surface and ambient atmospheric values)

where  $\varepsilon$  is the ration molecular weight of water to molecular weight of 'air' (= 0.622),  $\nu$  is the molecular heat conductivity of air,  $\nu$  is the kinematic viscosity of the air,  $\rho_{\rm o}$  is the density of the saturated air at the water surface temperature,  $ho_{\it surf}$  is the density of the surface water,  $\xi$ is a roughness correction coefficient for lake surface, a is the molecular heat diffusivity of air,  $C_o$  is the water vapour concentration of saturated air at the water surface,  $C_a$  is the water vapour concentration of the ambient air, e is the vapour pressure of saturated air, E is the height of water evaporated per unit time,  $N_{hr}$  is the number of seconds per hour and p is the total air pressure. The zero-wind evaporation power flux density is calculated as:

$$Q_{zero\ wind} = E\ \rho_{surf}\ \lambda\ /\ N_{hr} \tag{22}$$

#### 2.2.2.3 Wind-sheltering

Hipsey et al. (2003) presented a simple adjustment to the bulk transfer equation to account for the effect of wind-sheltering around small dams. The method employs the use of the shelter index which is well suited to one-dimensional application by accounting for the length scale associated with the vertical obstacle relative to the horizontal length scale associated with the dam itself. A modified form of the shelter index approximation has been implemented into DYRESM, which reduces the effective surface area for heat and momentum fluxes:

$$A_E = A \tanh\left(\frac{A}{A_C}\right) \tag{23}$$

where A<sub>C</sub> is the critical area defined empirically (Xenopoulos and Schindler, 2001).

# 2.3 Model Application

#### 2.3.1 Test sites

The test sites chosen for the study are intended to provide a broad cross-section of conditions typical of irrigation districts across the country. Four climatic regions were selected for the study: southeast Queensland, northern Victoria, southern South Australia, and southwest Western Australia. In each climate zone (except WA), several sizes of dam were also simulated. These are summarised in Table 1 and based on data supplied by Mr. Murray Chapman of NPSI, they reflect the 10<sup>th</sup>, 50<sup>th</sup> and 90<sup>th</sup> percentile in terms of dam volumes recorded for the respective regions.

Table 1: Outline of simulations conducted grouped according to the geographic regions they represent.

Location &			Bank Slope	Max Depth (m)	Surface Area (Ha)				
Climate Data	Code								
Queensland, Murray Darling Basin									
St George	QLD1	140.3	3:1	4.0	4.0				
St George	QLD2	358.1	3:1	4.0	9.7				
St George	QLD3	3148.1	3:1	4.0	80.9				
Northern Victoria									
Wangaratta	VIC1	1.98	3:1	4.0	0.11				
Wangaratta	VIC2	12.8	3:1	4.0	0.47				
Wangaratta	VIC3	41.1	3:1	4.0	1.28				
Southern South Australia									
Barossa	SA1	32.8	3:1	6.0	0.83				
Barossa	SA2	107.1	3:1	6.0	2.29				
Barossa	SA3	191.2	3:1	6.0	3.86				
Southwest Western Australia									
Witchcliffe	WA1	358.1	3:1	4.0	9.7				

#### 2.3.2 Morphometry

To generate the necessary morphometry data for DYRESM, it was assumed that all dams had the shape of an inverted truncated pyramid since this shape is typical of many excavated earth dams across Australia. Although there are numerous other types of dams (e.g. gully wall dams) that have shapes that are not square or rectangle, preliminary simulations with variable morphometry curves, showed almost negligible sensitivity; that is the evaporation estimates over this time scale is largely one-dimensional. This assumption is therefore not important for this evaporation analysis, but note that for specific water balance studies, the exact nature of the morphometry will need to be resolved.

For this geometry, surface area and volume are analytical functions of height following (Hipsey, 2003):

$$A(h) = \left(b + \frac{2h}{b_s}\right)^2 \tag{24}$$

$$V(h) = b^2 h + 2h^2 \frac{b}{b_s} + \frac{4h^3}{3b_s^2}$$
 (25)

where A is the surface area of the water surface (m<sup>2</sup>), V is the volume of water (m<sup>3</sup>), h is the depth of water (m), b is the base width (m) and  $b_s$  is the batter slope. The above expressions were used to generate dams whose maximum surface area and volume approximately matched data supplied by the client for the 30<sup>th</sup>, 50<sup>th</sup> and 90<sup>th</sup> percentiles (see Table 1). Curves relating height to area and volume are shown in Figure 4.

#### 2.3.3 Meteorological forcing

The Bureau of Meteorology (BoM) supplied the necessary meteorological data (air temperature, vapour pressure, wind speed) at hourly resolution for 2005 at the sites indicated in Table 1: St George, QLD; Wangaratta, VIC; Barossa Valley, SA, and Witchcliffe (near Margaret River), WA. Generally the supplied data was of good quality, but where periods of missing data were present they were in-filled based on interpolation of neighboring data. There were no extended periods of missing data, so the effect of this on the overall analysis is minimal.

No solar radiation data or cloud cover data were available from BoM for any of the sites, so synthetic data was constructed. For solar radiation the data was synthesised based on algorithms from the U.S. Naval Observatory, which estimate the incident radiation from latitude, longitude and time of year. Theoretical solar radiation values were mediated by the amount of clouds present, by assuming a linear attenuation and that 30% of light reaches the surface under a cloud cover of 1. Cloud cover values were estimated from available unpublished data from North Pine Dam in Queensland for St George, from Myponga Reservoir in South Australia for the Barossa, and from Lake Eildon in New South Wales for northern Victoria. The average values of the historical data were approximately 0.4 for QLD and SA, 0.6 for VIC and 0.5 was estimated for southwest WA, and these were assumed to be constant over the course of the year. Rainfall was not included directly, but its role accounted for in the inflows, discussed below.

The final data used for DYRESM is shown in Figure 5(a-d).

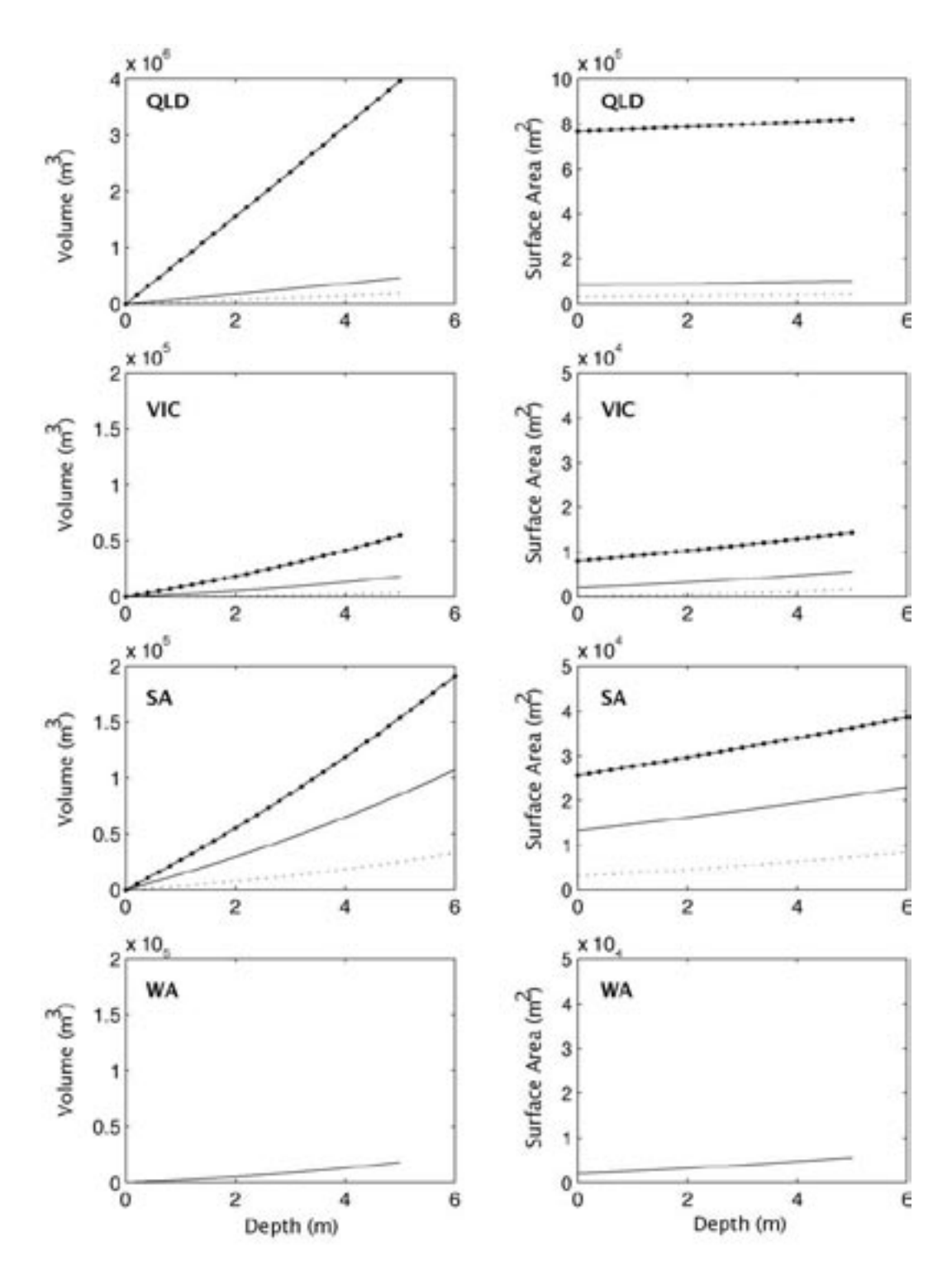


Figure 4: Relationship between the depth, surface area and volume of the 10 simulated dams (three each for QLD, VIC and SA climates, and one for WA). Curves calculated from Eqs. 24-25.

# 2.3.4 Water balance

Since this is a hypothetical study it was not our aim to model any actual dams, but to simulate typical behavior and use this as the basis for the evaporation analysis. It was therefore necessary to artificially control the water balance so that it reflected "normal" operation and so that it was consistent between the test sites. This was achieved by enforcing the following criteria:

- Initial conditions were set to be one metre below the maximum;
- Water level at the end of the year must be equal to that at the beginning of the year;
- All inflows to the dam occurred over the winter months during 8 discrete events;
- Withdrawals occurred throughout the year, but significantly more was drawn upon during the summer months (defined as the first and last 60 days of the year).

By following these assumptions we were able to reasonably simulate the annual variation in volume, area and depth that may be expected. Because of the size and dimension differences between the dams, the withdrawal and inflow volumes were calculated to enforce the second criterion listed above.

Note that since the rainfall patterns will vary between the climatic zones the use of the third assumption may cause seasonal water level trends to vary from that typically experienced in the relevant location. However, since the aim of this report is to focus on the evaporation mechanism, it was necessary to "normalize" the various sites water balance to negate any interacting effects. Preliminary simulations showed little sensitivity to water level so this is not deemed to be an important factor. For dedicated water balance investigations, then more appropriate estimates of rainfall, and inflows will be essential.

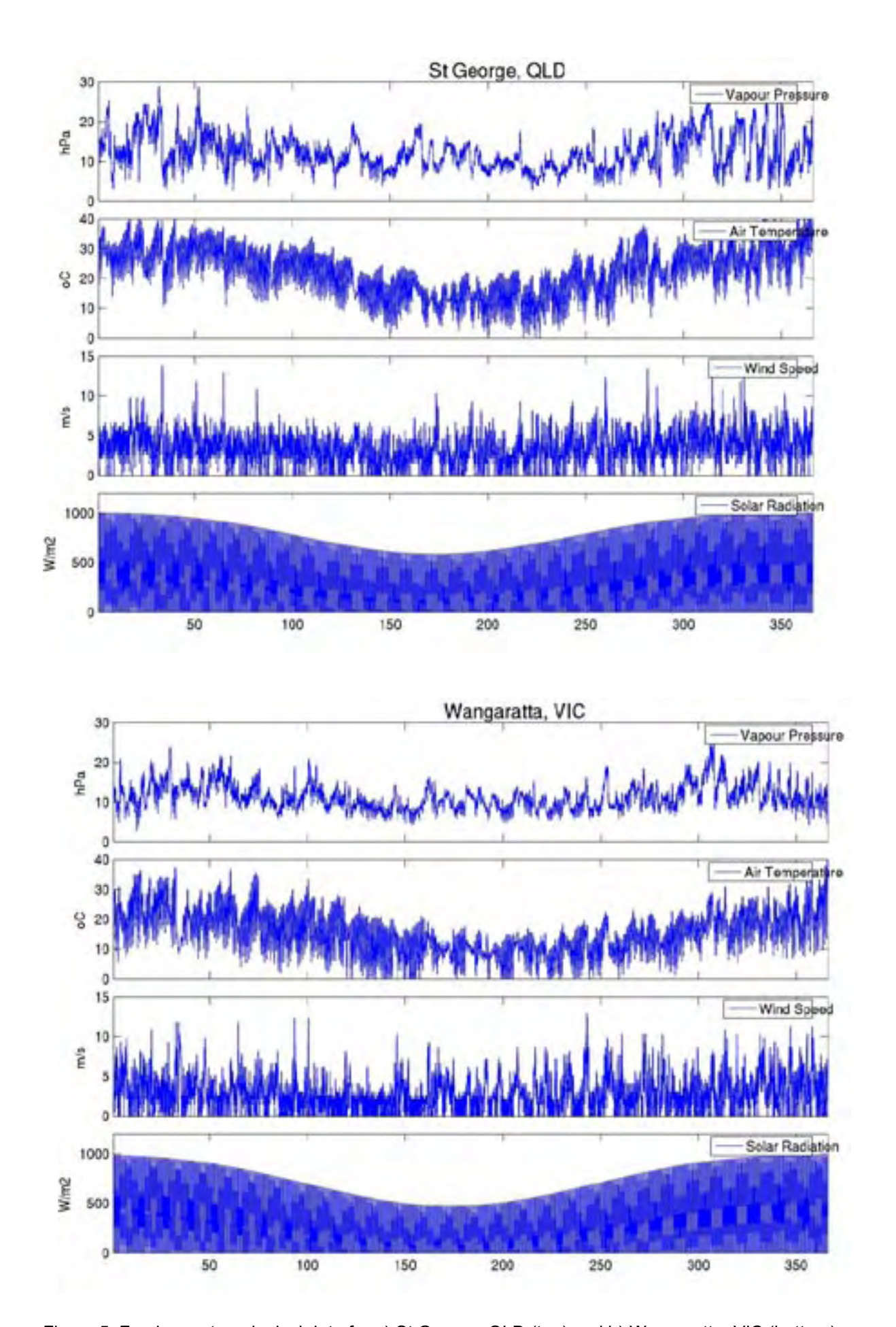


Figure 5: Forcing meteorological data for a) St George, QLD (top) and b) Wangaratta, VIC (bottom).

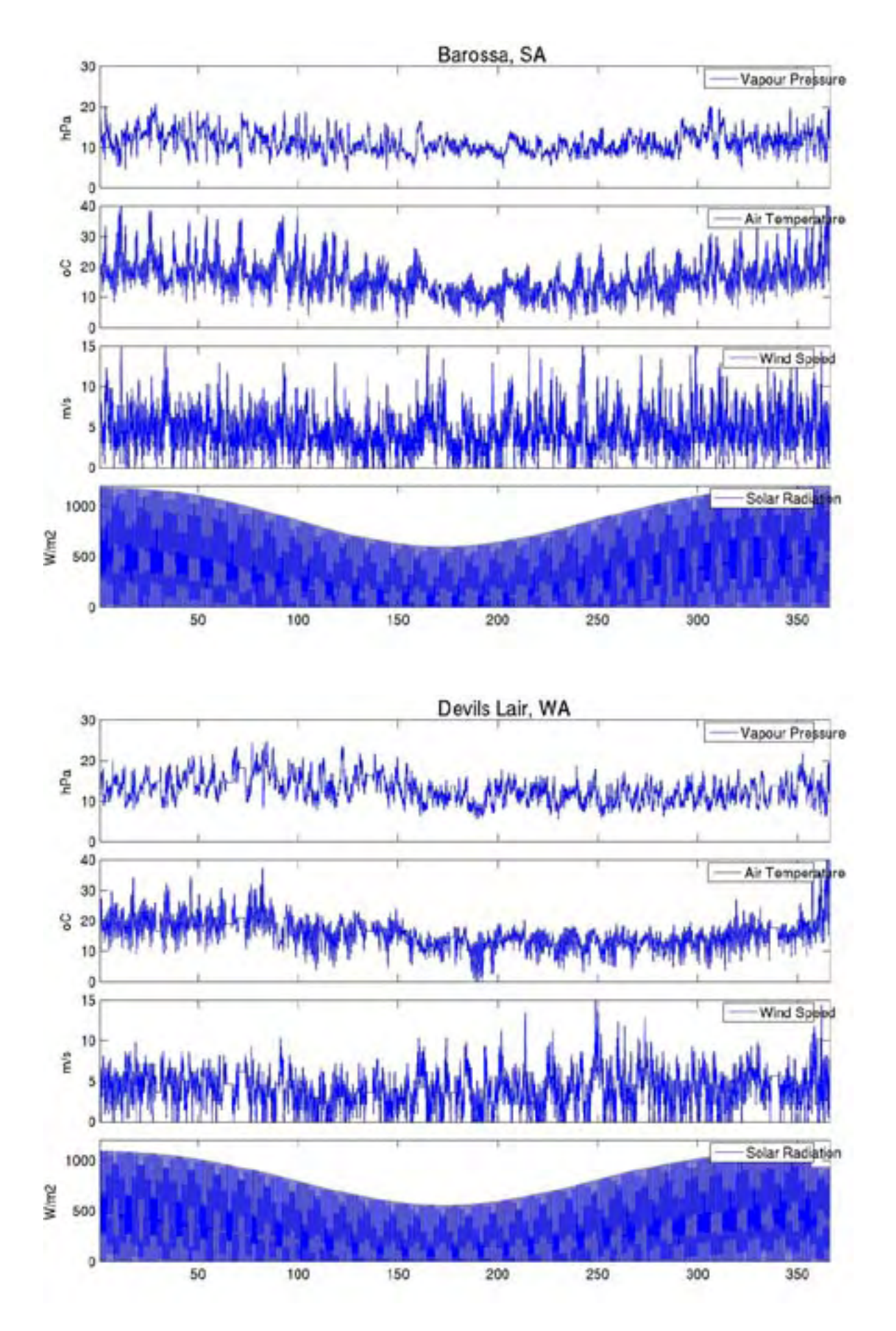


Figure 5(cont): Forcing meteorological data for c) Barossa, SA (top) and d) Devil's Lair, WA (bottom).

# 2.4 Configuration details

A unique simulation was created for each of the 10 scenarios outlined in Table 1. Each of the simulations had identical configuration parameters other than the specific differences in meteorology, morphometry, and water balance as outline above.

The time step of each simulation was set to hourly, and run from ordinal date 2005001 to 2005365.99. The extinction coefficient was set 2.0 - this is based on the generally high colour and turbidity seen in these storages. Minimum and maximum layer thicknesses were set to be 0.2 and 0.5m respectively, and the outlet height was set to be at a depth of 1.5m from the bottom. The meteorological data was assumed to be based at a fixed 6m above the dam base, estimated to be approximately 2m above the water surface. Leakage from the dams was assumed to be negligible.

The neutral bulk aerodynamic coefficient for momentum transport was set to 1.3 x 10<sup>-3</sup>, the shortwave albedo was set to 0.08, emissivity was set to 0.96 (Imberger and Patterson, 1981), the benthic boundary layer (BBL) dissipation coefficient was set to 1.4 x 10<sup>-5</sup> (Yeates and Imberger, 2003) and the vertical mixing coefficient was set to 200 (Yeates and Imberger, 2003).

# RESULTS

#### 3.1 Simulation results

To compare the different simulations output was analysed to examine the water column temperature structure, the surface temperature and atmospheric stability (through the Monin-Obukhov length), and the magnitude of the evaporative flux (Figure 6). The results highlight several key behaviors highlighted in turn next.

#### 3.1.1 Water column stratification

The seasonal variation in temperature is largely based on the climatic regime: the QLD dams vary between 10-30°C, the VIC dams vary between 5-25°C, the SA and WA dams vary between 10-25°C.

The patterns of water body stratification generally all follow a similar monomictic cycle. Although the depths are shallow, the high extinction coefficients and frequent periods of low wind allow the development of a strong (5-15°C) thermocline in the summer months. Higher winds, convective cooling and large inflows in winter result in a well-mixed system. The exception is the largest of the 10 simulated dams, QLD3 (3148 ML), since the large surface area was sufficient enough to allow negate the sheltering effects caused by local topography. As a result, the increased momentum input at the surface was able to create a well-mixed water column even during summer. Note that this is the typical of the temperature structure that would be experienced by all the dams if the wind-sheltering algorithms were not employed.

#### 3.1.2 Atmospheric instability

A prominent feature seen in all of the simulations was the dominance of significantly unstable atmospheric conditions, with z/L often hitting the maximum of -15. The comparison of surface water temperature and air temperature shows that the water is significantly warmer than the atmosphere for large periods of the day throughout the entire year. Such conditions encourage heightened convective transport from the water surface to the atmosphere and enhance the evaporative flux.

The trend is most prominent in the VIC, SA and WA simulations, which exhibit between 80-82% of all simulated hours throughout the year with z/L < -0.5. The QLD simulations showed a lower frequency of instability, around 59%.

#### 3.1.3 Evaporative flux rates

The top panel of the plots in Figure 6 show the evaporative flux rate (m day<sup>-1</sup>) at hourly and daily intervals for the entire year. The fluxes are highly variable in response to wind, humidity and temperature gradients between the water and atmosphere.

The daily integrated rates show that for the QLD simulations that the rates vary between 5 – 15 mm day<sup>-1</sup> in summer, but the hourly figures highlight the strong variability seen through the day. In winter, the evaporative fluxes are markedly lower, ranging from 2 - 5 mm day<sup>-1</sup>. and the magnitude of the daily variability much less. The pattern is consistent across the small, medium and large morphometries.

The daily integrated rates for the VIC simulations show similar trends, but the magnitudes are lower; 5 – 10 mm day<sup>-1</sup> during summer and <3 mm day<sup>-1</sup> during winter. The SA and WA simulations lie ion between these two extremes.

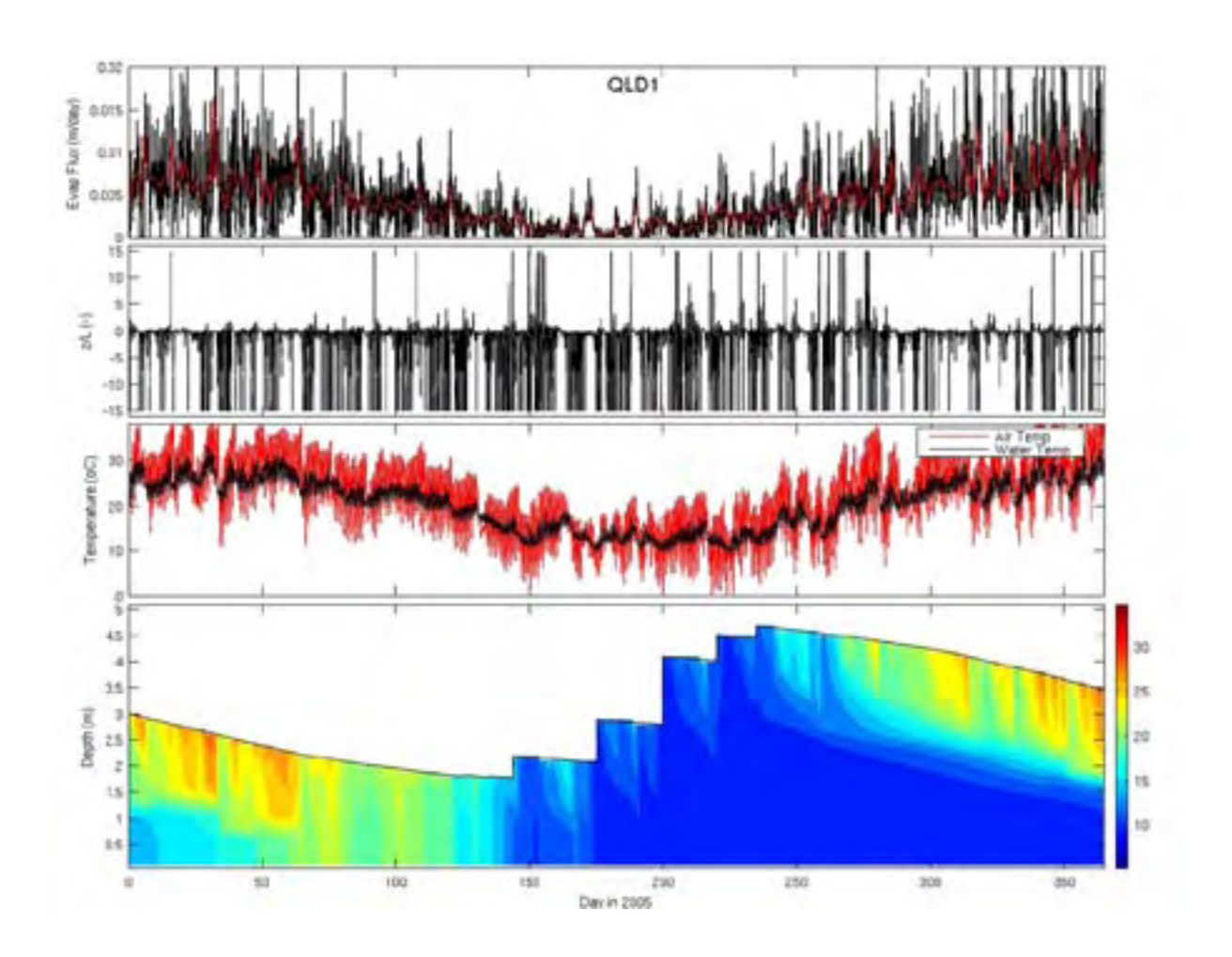


Figure 6a: DYRESM output showing hourly and daily evaporative flux (black and red lines respectively, top panel; m day<sup>-1</sup>), atmospheric stability (top-centre panel), surface and air temperatures (bottom-centre panel) and the water column thermal structure (bottom panel) as a function of time for simulation QLD1 (St George meteorological data, large morphometry).

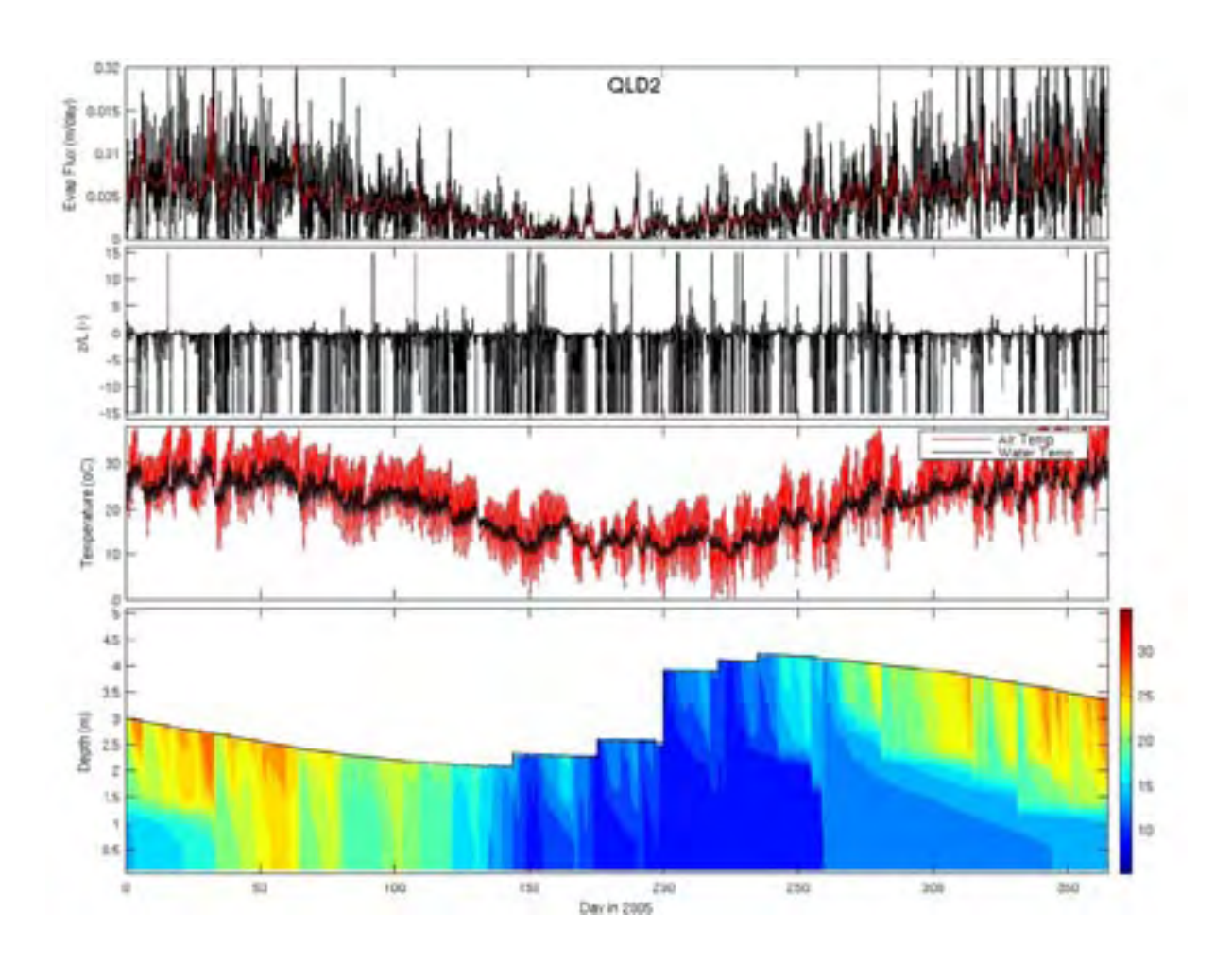


Figure 6b: DYRESM output showing hourly and daily evaporative flux (black and red lines respectively, top panel; m day<sup>-1</sup>), atmospheric stability (top-centre panel), surface and air temperatures (bottom-centre panel) and the water column thermal structure (bottom panel) as a function of time for simulation QLD2 (St George meteorological data, large morphometry).

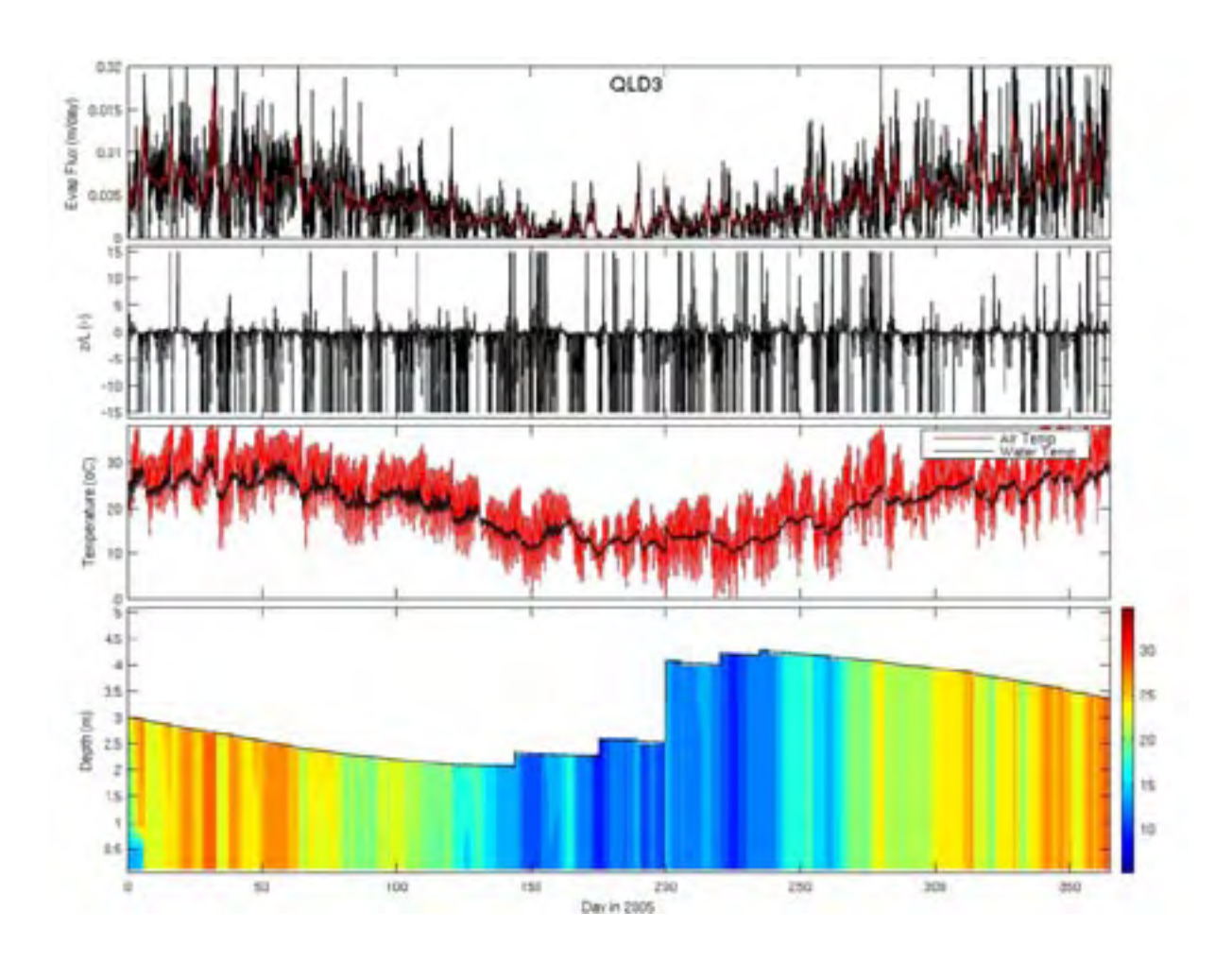


Figure 6c: DYRESM output showing hourly and daily evaporative flux (black and red lines respectively, top panel; m day<sup>-1</sup>), atmospheric stability (top-centre panel), surface and air temperatures (bottomcentre panel) and the water column thermal structure (bottom panel) as a function of time for simulation QLD3 (St George meteorological data, large morphometry).

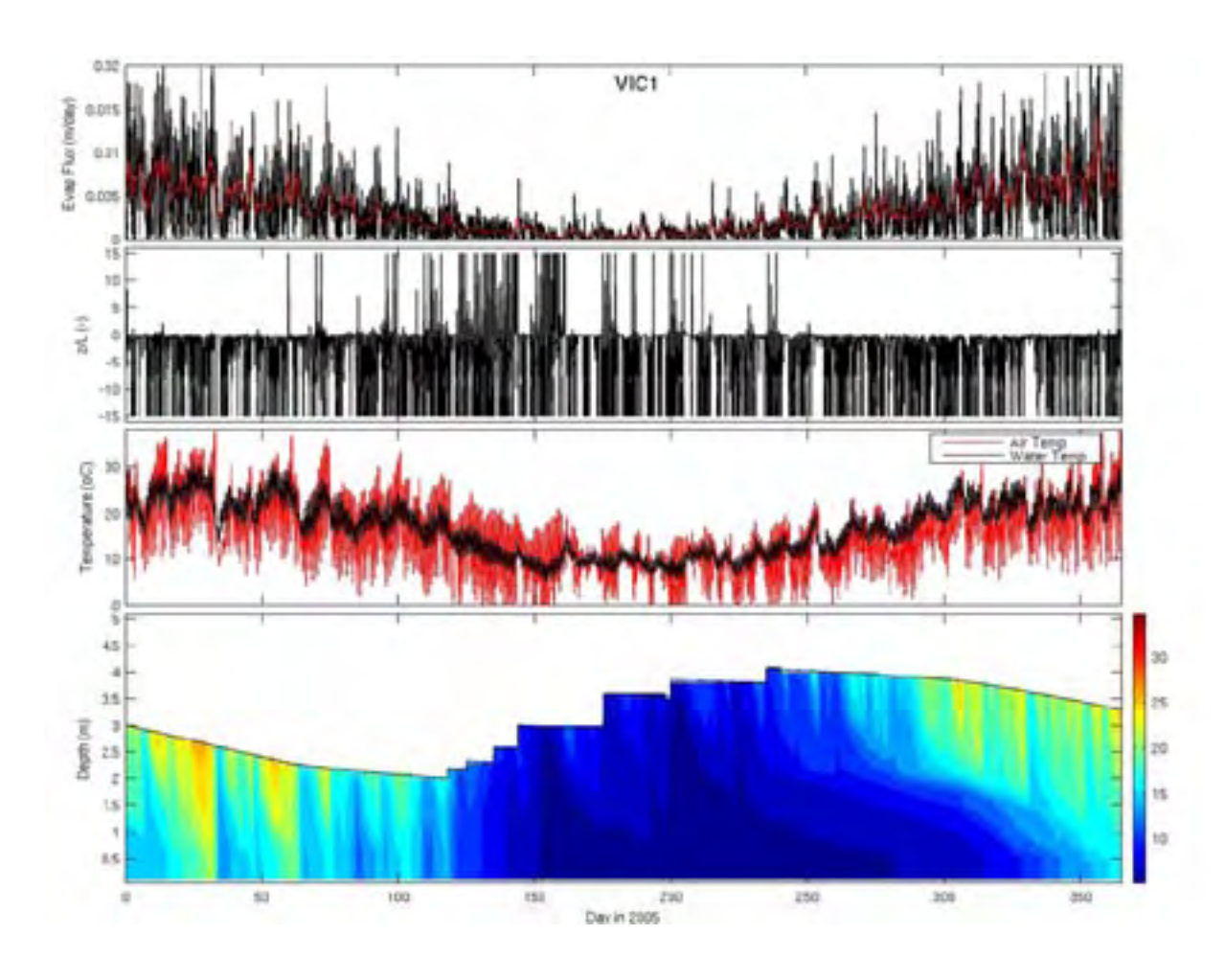


Figure 6d: DYRESM output showing hourly and daily evaporative flux (black and red lines respectively, top panel; m day<sup>-1</sup>), atmospheric stability (top-centre panel), surface and air temperatures (bottom-centre panel) and the water column thermal structure (bottom panel) as a function of time for simulation VIC1 (Wangaratta meteorological data, small morphometry).

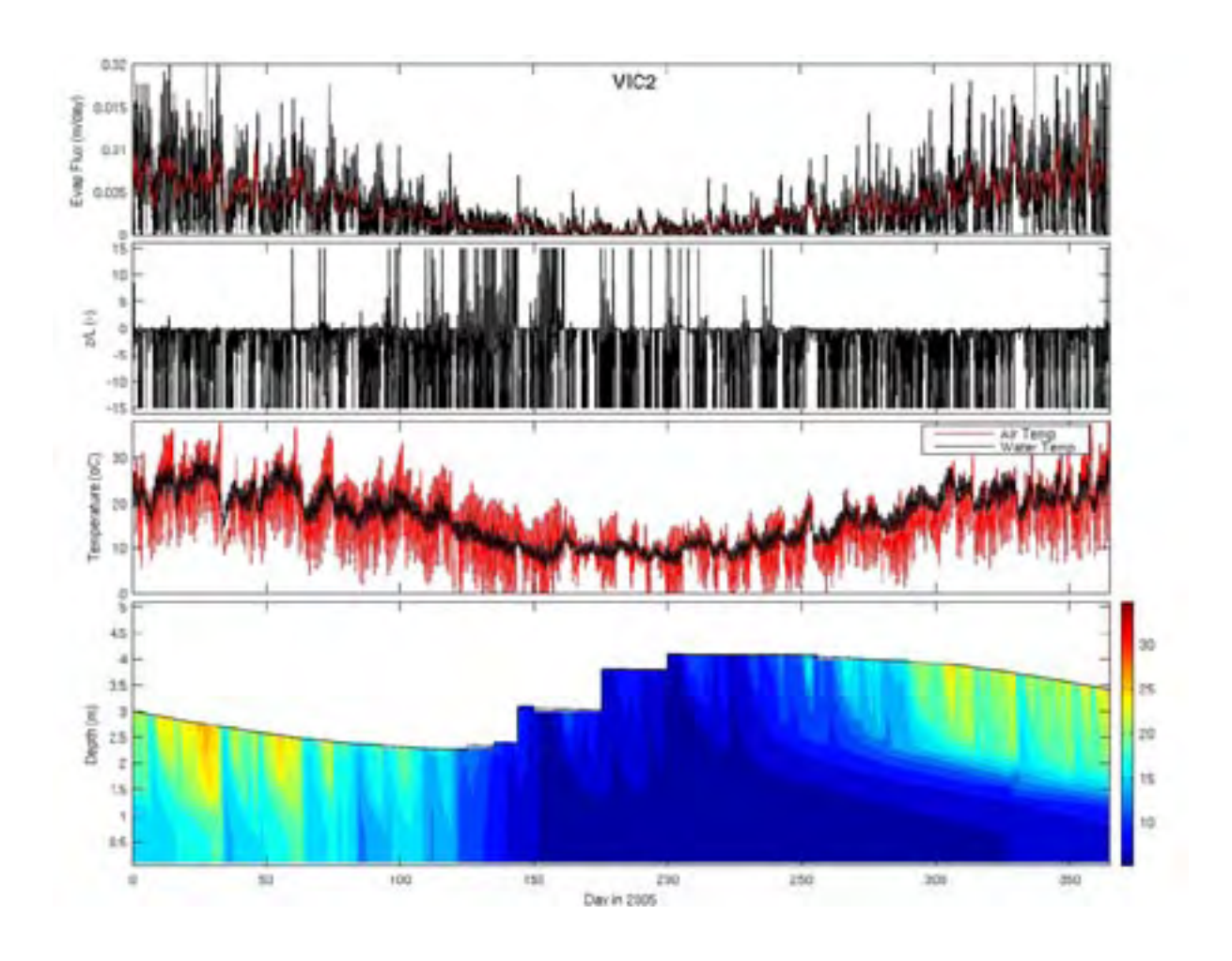


Figure 6e: DYRESM output showing hourly and daily evaporative flux (black and red lines respectively, top panel; m day<sup>-1</sup>), atmospheric stability (top-centre panel), surface and air temperatures (bottom-centre panel) and the water column thermal structure (bottom panel) as a function of time for simulation VIC2 (Wangaratta meteorological data, medium morphometry).

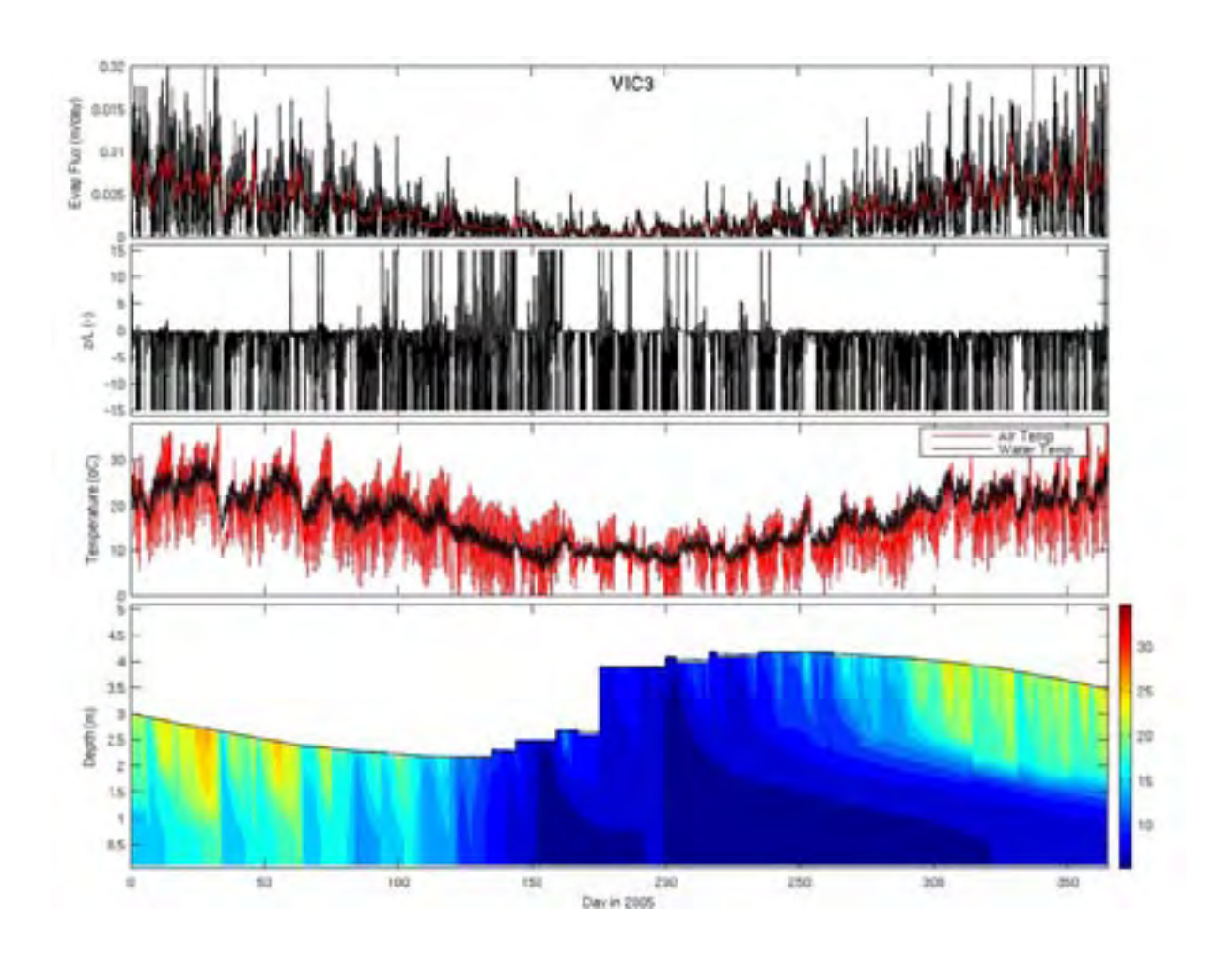


Figure 6f: DYRESM output showing hourly and daily evaporative flux (black and red lines respectively, top panel; m day<sup>-1</sup>), atmospheric stability (top-centre panel), surface and air temperatures (bottomcentre panel) and the water column thermal structure (bottom panel) as a function of time for simulation VIC3 (Wangaratta meteorological data, large morphometry).

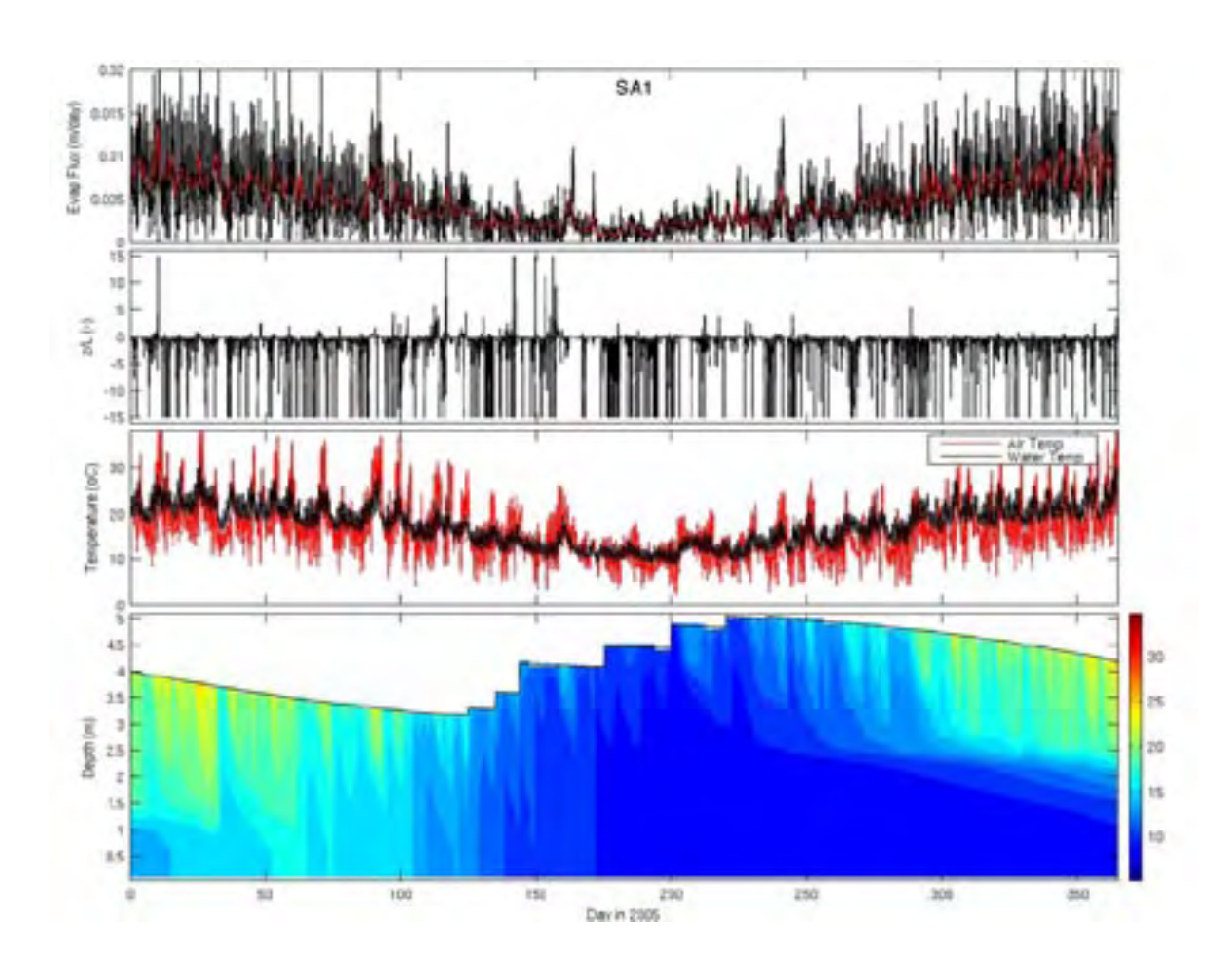


Figure 6g: DYRESM output showing hourly and daily evaporative flux (black and red lines respectively, top panel; m day<sup>-1</sup>), atmospheric stability (top-centre panel), surface and air temperatures (bottom-centre panel) and the water column thermal structure (bottom panel) as a function of time for simulation SA1 (Barossa meteorological data, small morphometry).

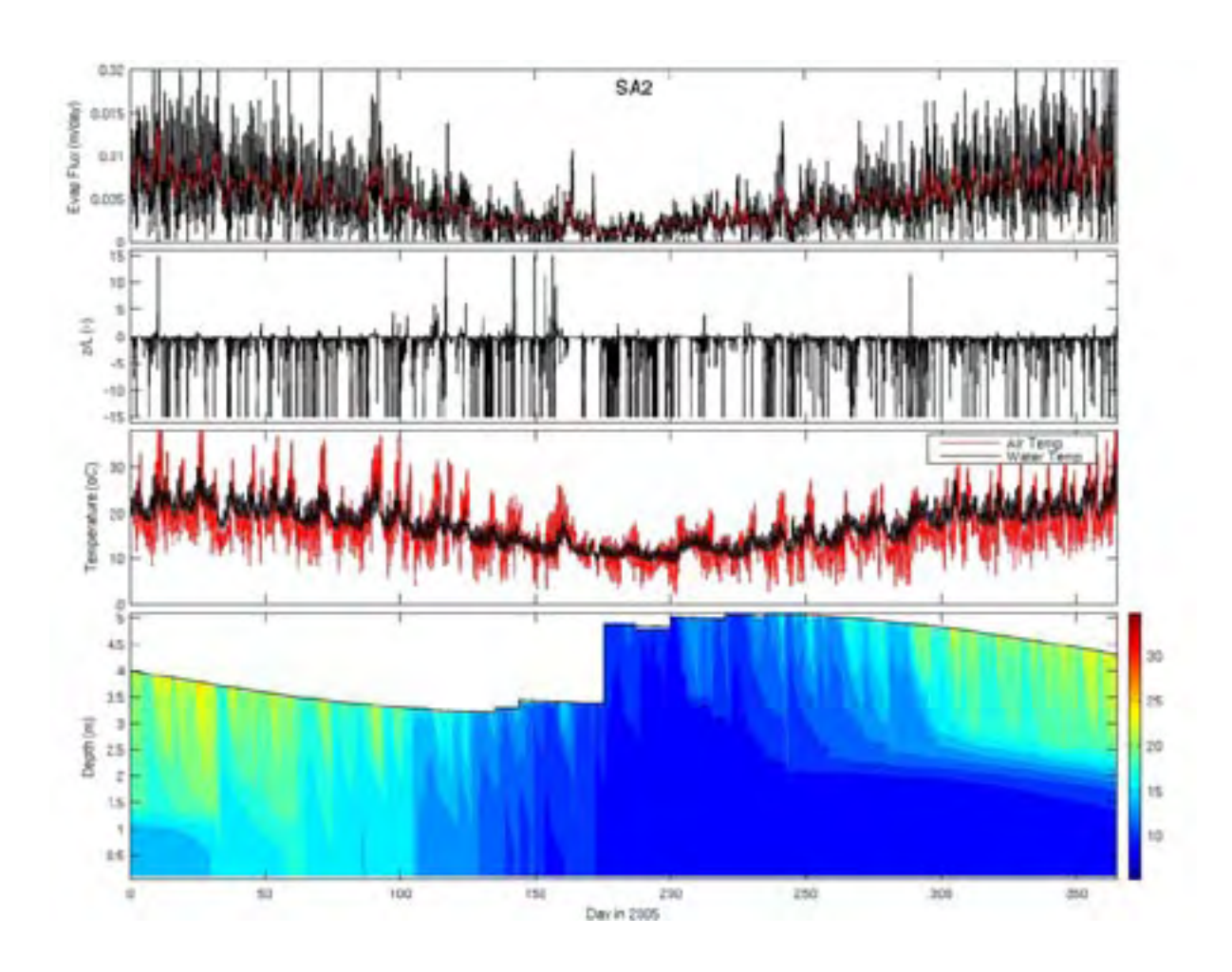


Figure 6h: DYRESM output showing hourly and daily evaporative flux (black and red lines respectively, top panel; m day<sup>-1</sup>), atmospheric stability (top-centre panel), surface and air temperatures (bottom-centre panel) and the water column thermal structure (bottom panel) as a function of time for simulation **SA2** (Barossa meteorological data, medium morphometry).

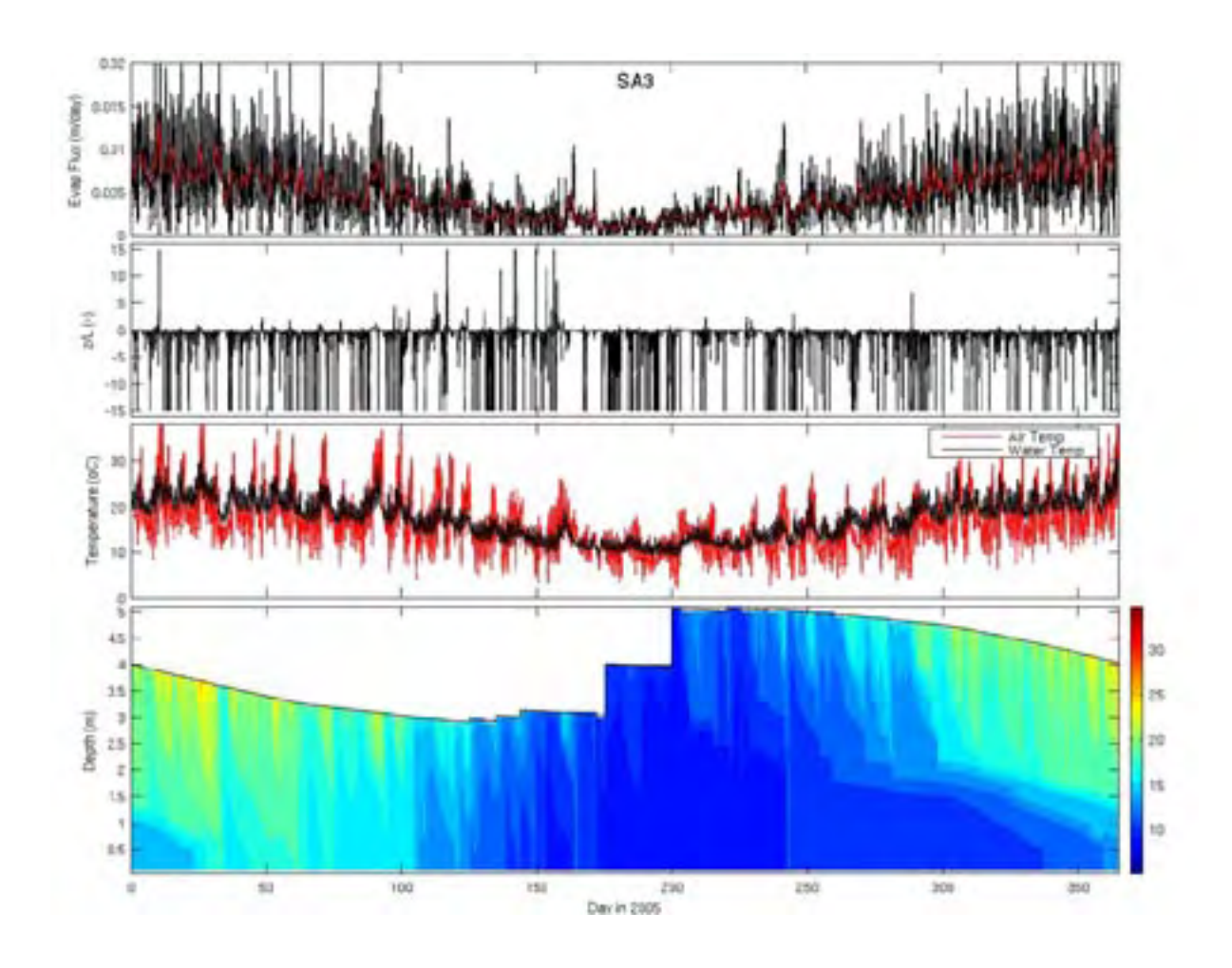


Figure 6i: DYRESM output showing hourly and daily evaporative flux (black and red lines respectively, top panel; m day<sup>-1</sup>), atmospheric stability (top-centre panel), surface and air temperatures (bottomcentre panel) and the water column thermal structure (bottom panel) as a function of time for simulation SA3 (Barossa meteorological data, large morphometry).

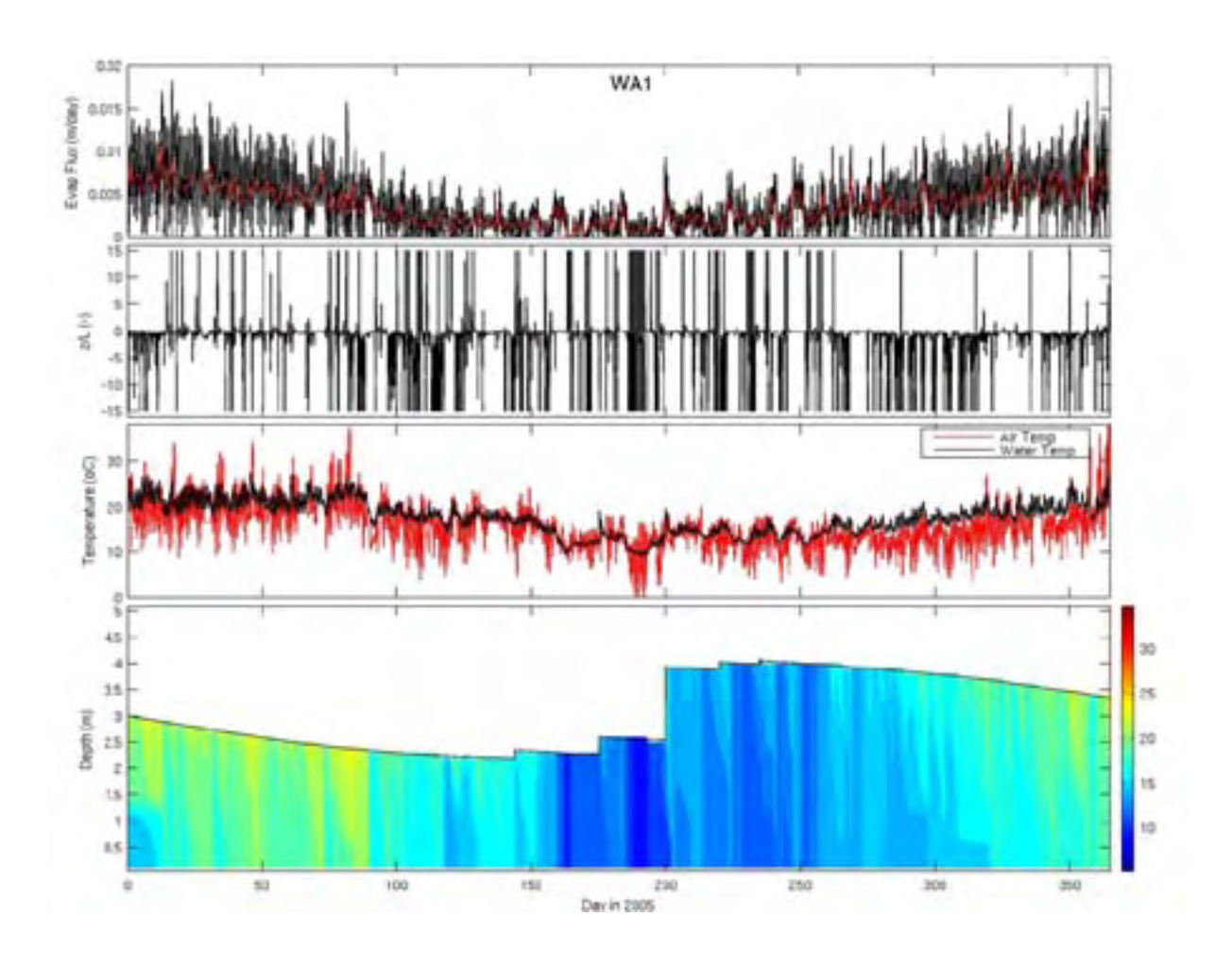


Figure 6j: DYRESM output showing hourly and daily evaporative flux (black and red lines respectively, top panel; m day<sup>-1</sup>), atmospheric stability (top-centre panel), surface and air temperatures (bottomcentre panel) and the water column thermal structure (bottom panel) as a function of time for simulation **WA1** (Witchcliffe meteorological data, medium morphometry).

# 3.2 Evaporation analysis

Annual evaporation rates (Table 2) vary considerably between the different climatic zones, with the QLD simulations averaging 1.62 m yr<sup>-1</sup>, the VIC simulations averaging 1.17 m yr<sup>-1</sup>, the SA simulations averaging 1.71 m yr<sup>-1</sup>, and WA predicting 1.31 m yr<sup>-1</sup>. These compare well with long-term mean annual potential evaporation rates published by BoM (1.9, 1.4, 1.8 and 1.4 m yr<sup>-1</sup> for the four locations respectively), once corrected for the pan-lake factor, and bearing in mind that the simulated year may have departed from "average" meteorological conditions and also the synthetic nature of the shortwave and cloud cover data. In all cases, only very limited variation was predicted between the different sized dams forced with the similar meteorology.

Despite the large variability between evaporation totals, there was little variability between the fraction of evaporation which occurred during night time (defined as the period where incoming solar radiation was less than 20 W m<sup>-2</sup>) and that during the day (Table 2). The average night time evaporation fraction was 45% for the QLD simulations, 43% for the VIC simulations, 41% for the SA simulations, and 36% for the WA simulation.

Table 2: Total evaporation predicted for the 10 simulated dams, showing the percentage of evaporation proportioned between day and night.

	QLD1	QLD2	QLD3	VIC1	VIC2	VIC3	SA1	SA2	SA3	WA1
Total (m)	1.631	1.614	1.606	1.168	1.179	1.180	1.708	1.712	1.705	1.308
Day (%)	55.7	55.7	54.6	57.7	57.1	57.0	59.5	59.4	59.2	64.0
Night (%)	44.3	44.3	45.4	42.3	42.9	43.0	40.5	40.6	40.8	36.0

The simulations were further investigated by examining the intra-annual variability in the night time fraction,  $E_N/E_T$  (Figure 7). In all four climatic zones the night time evaporation fraction displays a strong seasonal trend, with the minimum fraction in summer and the maximum in winter. Note this should be considered in light of the appreciable decrease in evaporation during the cooler months. The fraction varies from 40% in the summer to 57% in the winter for the QLD simulations, from 30 - 70% for the VIC simulations, from 30 - 65% for the SA simulations and from 30 - 55% for the WA simulation.

Except for the QLD simulations, there was negligible difference predicted between the small, medium and large dam morphometries. Although the seasonal trend was identical for the three QLD simulations, the magnitude of the night time fraction was noticeably higher for

QLD3, presumably as a result of the different thermal structure of the water body, as indicated previously.

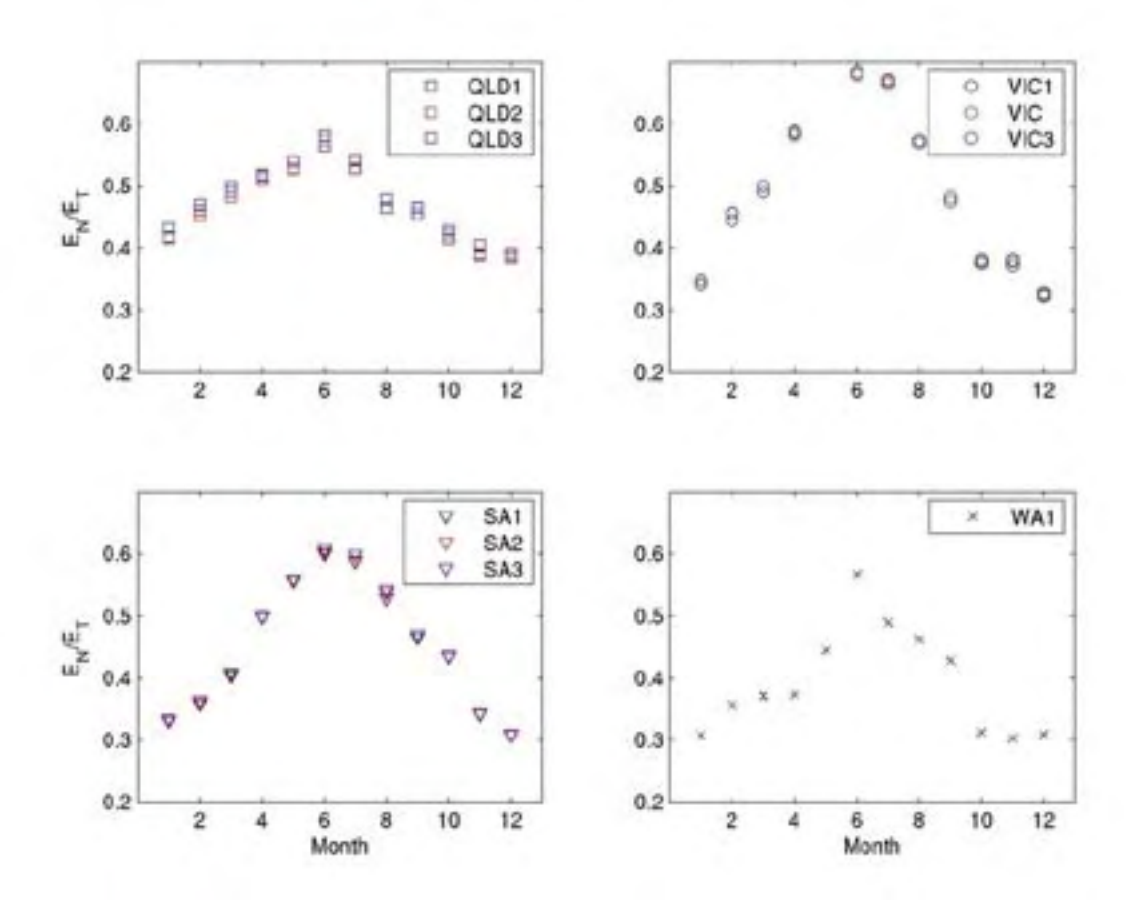


Figure 7: Intra-annual variability in night time evaporation (E<sub>N</sub>), as a fraction of the total monthly evaporation  $(E_T)$ , for the 4 climatic regions simulated.

To further characterise the predicted variability in night time evaporation rates, the importance of low wind conditions, unstable conditions and combined unstable + low wind conditions was examined in more detail for each simulation (Figure 8). Low wind periods occurred between 1 - 25% of the time, and surprisingly, all climates displayed a higher fraction of low wind periods during the winter months. SA exhibited the highest wind speeds of all the climates with the low wind speed fraction peaking at <10% of the time. Although this does not demonstrate a causal relationship, the pattern observed in low wind speeds and night time evaporation dominance in the winter months suggests the higher night time evaporation fraction is a result of heightened atmospheric instability. However, as shown in Figure 8b, there is no clear relationship between persistence of local atmospheric instability and the night time evaporation fraction. In fact, the trend is reversed and at least for VIC, SA and WA, the winter is the most stable time of the year. Nonetheless, if the fraction of time that the water body experiences low wind AND unstable conditions is calculated (Figure 8c),

then it closely resembles the low wind plot (Figure 8a). This suggests that when low wind conditions prevail, the local boundary layer is predominantly unstable.

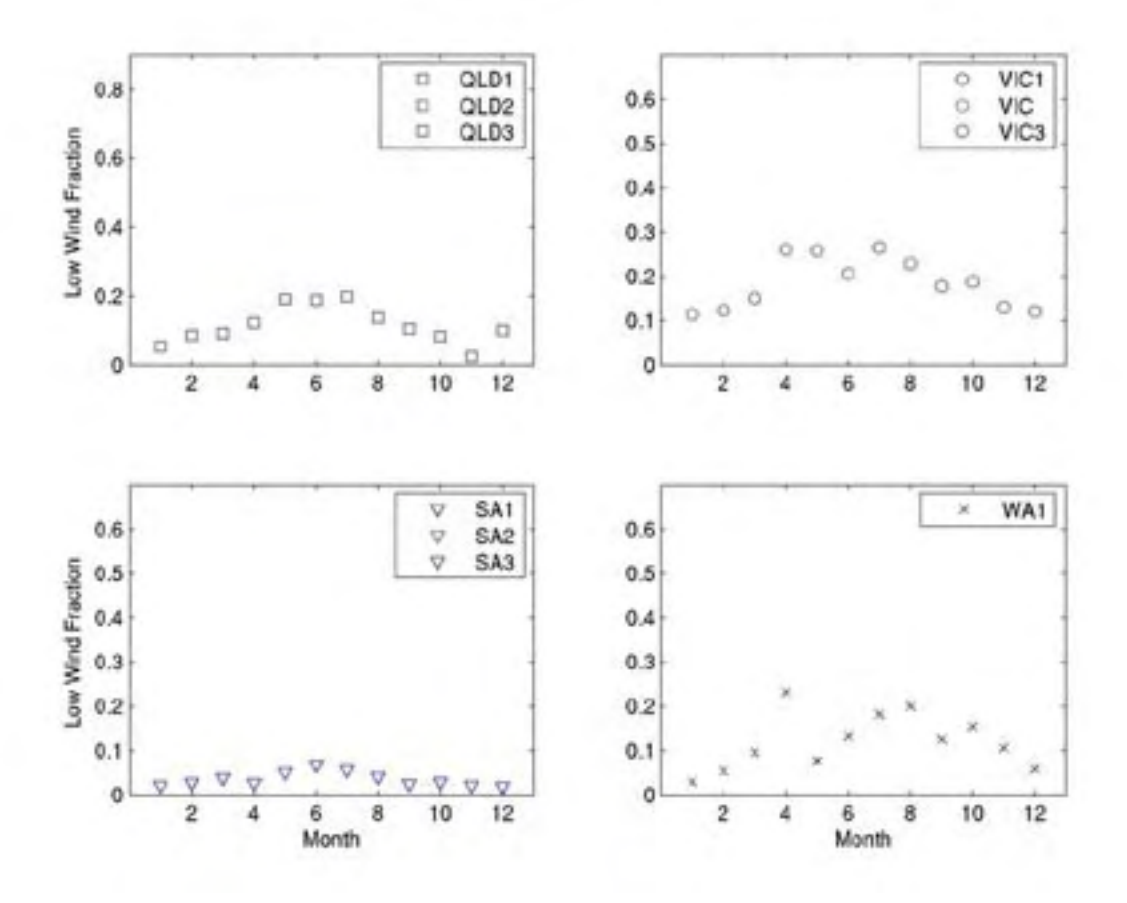


Figure 8a: Intra-annual variability in the fraction of the month that experienced low wind speeds (<1 m s<sup>-1</sup>) for the 4 climatic regions simulated (difference between morphometries indistinguishable due to identical wind forcing for each).

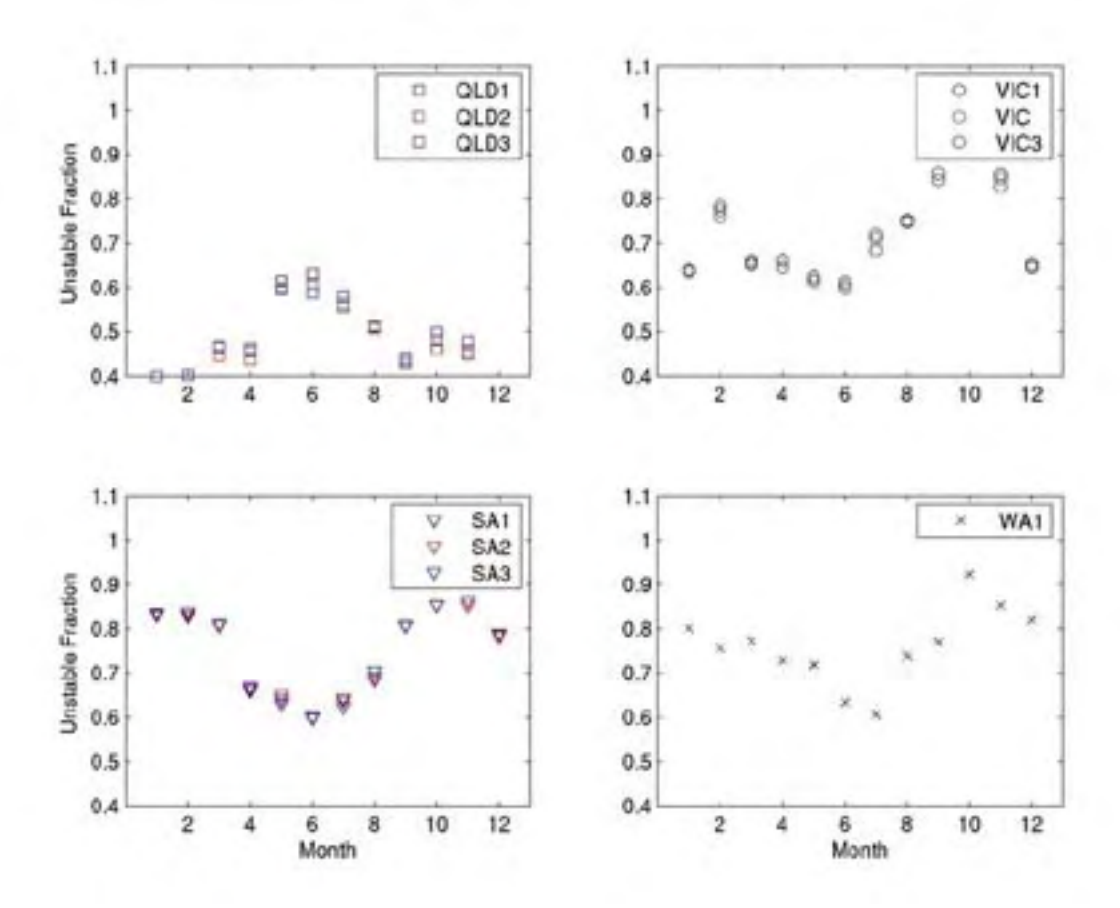


Figure 8b: Intra-annual variability in the fraction of the month that experienced unstable conditions  $(z/L < -0.5 \text{ m s}^{-1})$  for the 4 climatic regions simulated.

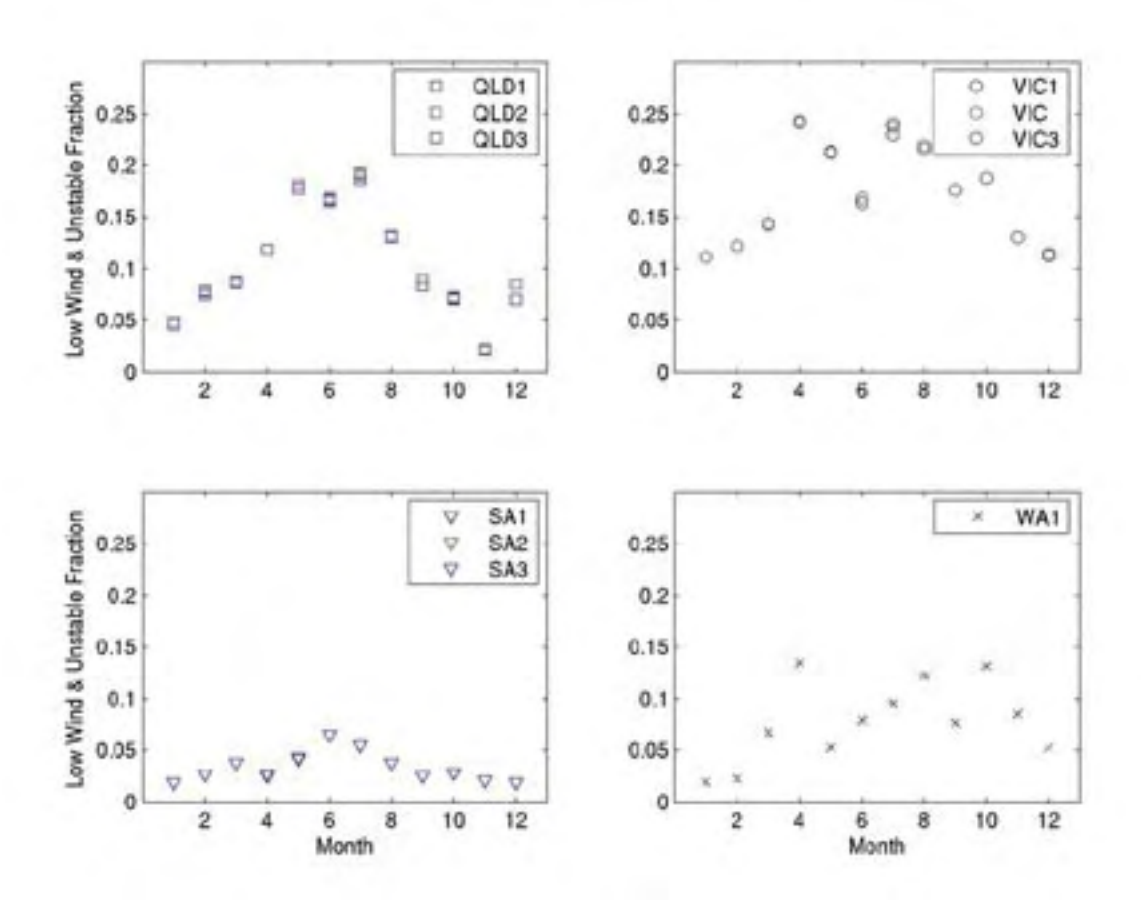


Figure 8c: Intra-annual variability in the fraction of the month that experienced both low wind (<1 m s<sup>-1</sup>) and unstable  $(z/L < -0.5 \text{ m s}^{-1})$  conditions for the 4 climatic regions simulated.

We can infer from these trends that the reason the night time fraction of evaporation increases during the winter months is because of enhanced free convection over the water during extended periods of low wind and local instability. That is not to say that this process is not also important during the summer months; one should bear in mind that the actual magnitude of the night time evaporative flux is much higher during the summer months and it is just the relative contribution of the night time evaporation component to the over all loss that is heightened in winter.

An unexpected result was obtained when comparing the monthly average night time wind speed with the night time evaporation fraction (Figure 9). Here the four different climatic regions differed considerably, with QLD exhibiting a negative correlation between night time wind and evaporation fraction, VIC showing no correlation, and SA and WA showing a positive correlation. The result from the QLD data is consistent with the conclusion outlined above, but the occurrence of positive correlations in the SA and WA datasets suggests the

dominance of night time evaporation during the winter months is in fact due to both increased free convection and increased forced convective losses.

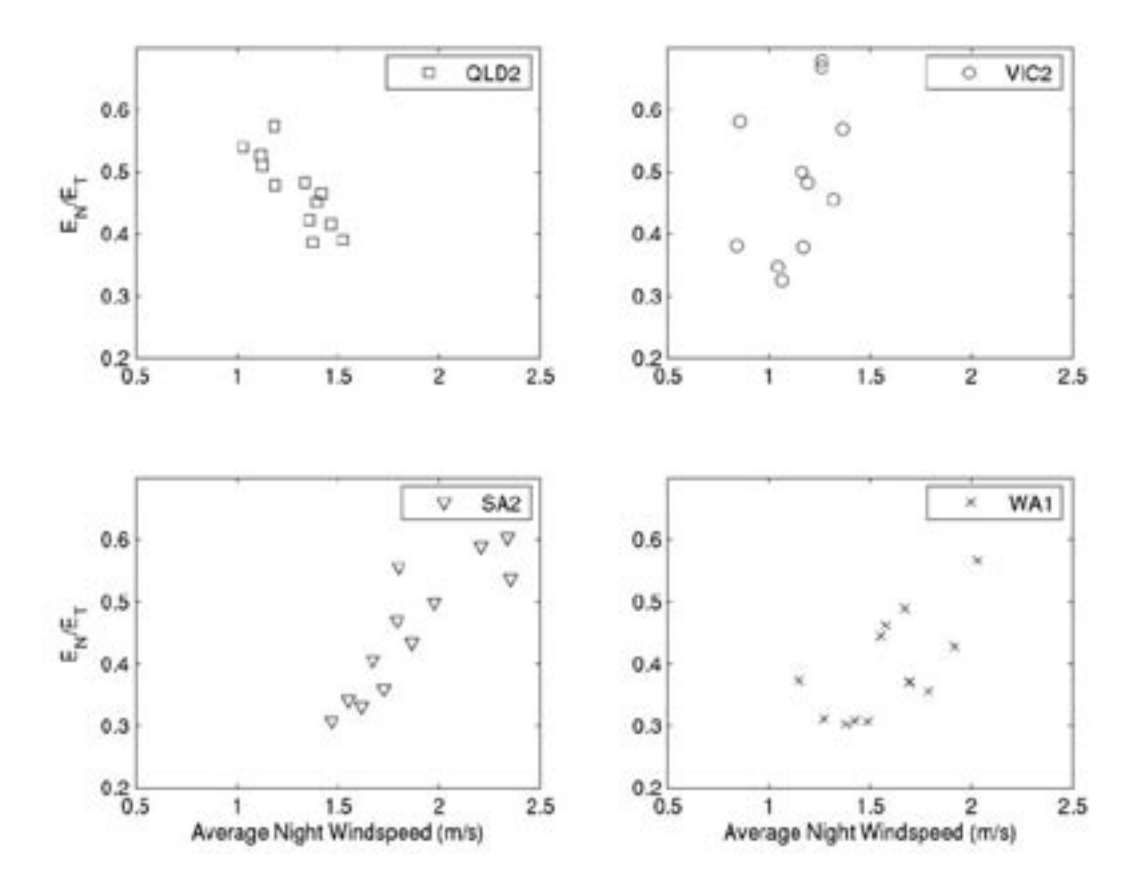


Figure 9: Relationship between the average night time wind speed and the night time evaporation fraction (E<sub>N</sub>/E<sub>T</sub>) for the 4 climatic regions simulated (as indicated by the mid-size dam simulation for QLD, VIC and SA).

## 3.3 Model comparison with existing methodology

To ascertain the significance of the non-neutral atmospheric stability (AS), still-air and windsheltering (WS) corrections to the evaporative flux algorithms, identical simulations to those outlined above were run but with the simplified flux calculation methodology (i.e. equations 1 -3 were employed using a constant bulk-transfer value). Note that this comparison assumes the existing methodology would couple the evaporation equation outlined in Watts (2005) to a hydrodynamic model with the sophistications of DYRESM for estimation of the surface temperatures. Where other methods are used to determine the surface water body temperature, then the results would be expected to differ more considerably.

The results of this comparison indicate that the role of the correction is modest in terms of affecting the prediction of the overall magnitude of the evaporative flux (Table 3). Differences

between the methodologies range between -5.1% - 1.6% for the 10 simulations (relative to the AS and WS corrected simulations), which is low compared to the uncertainties in other aspects of the water balance.

The differences are more pronounced when comparing the fraction of evaporation that occurs during the night, ranging from -5.7 - 16.1%. With the exception of the 1 WA simulation, the uncorrected flux equations tend to under predict the role of the night time evaporative loss, which is consistent with the above analysis. Nonetheless, we conclude that the existing bulk-transfer equation based on a neutral transfer coefficient is a suitable methodology, at least for long time integrations, and assuming suitable prediction of water body surface temperatures.

Table 3: Comparison of total evaporation and percentage of evaporation proportioned between day and night for the 10 simulated dams, using DYRESM with and without the atmospheric stability (AS) and wind scaling (WS) corrections.

	QLD1	QLD2	QLD3	VIC1	VIC2	VIC3	SA1	SA2	SA3	WA1
With AS + WS:										
Total (m)	1.631	1.614	1.606	1.168	1.179	1.180	1.708	1.712	1.705	1.308
Day (%)	55.7	55.7	54.6	57.7	57.1	57.0	59.5	59.4	59.2	64.0
Night (%)	44.3	44.3	45.4	42.3	42.9	43.0	40.5	40.6	40.8	36.0
No AS or WS:										
Total (m)	1.673	1.679	1.688	1.153	1.165	1.166	1.685	1.689	1.682	1.287
Day (%)	62.2	61.9	61.9	62.8	62.7	62.7	61.3	61.3	61.3	62.0
Night (%)	37.8	38.1	38.1	37.2	37.3	37.3	38.7	38.7	38.7	38.0

#### 4 **DISCUSSION & CONCLUSIONS**

### 4.1 Role of night time evaporation

Irrespective of a dam's size or the climatic region it is located in, the contribution of evaporation during the night is considerable. Predictions from this study using 10 test dams in four different climatic regions suggest that between 35 - 45% of the total annual loss of water through evaporation was during the night - in a climate where potential evaporation is approximately 1.5 m year<sup>-1</sup>, the night time fraction equates to roughly 0.6 m year<sup>-1</sup>. This is supported by the detailed simulations presented in Hipsey et al. (2004) who used a full 2D aerodynamic model to simulate the surface fluxes over the course of two days, and compared the daily integrations with observed data. Webster and Sherman (1995) also performed detailed heat budget calculations from a fetch-limited water body and presented daily cycles of evaporation from which it was estimated that approximately 40-50% occurs outside of daylight hours. Imberger and Patterson (1991) used a similar methodology for estimating surface fluxes from measured data from a moderate sized reservoir in southwest Western Australia and also predicted values between 30-50% during the evening.

Bearing in mind that this was a purely numerical study examining the relative difference in behaviors of realistic but idealized study sites, it was observed that most of the variability seen in the night time evaporation fraction was due to climate. Southwest WA displayed the lowest night time contribution (36%) and Murray-Darling Basin region of Queensland showed the highest (44%). Both northern Victoria and the Barossa region of SA showed contributions of approximately 40% over the simulated year. Nonetheless, the analysis highlights the night time evaporation should be considered equally important across all irrigation districts across Australia, regardless of climatic zone.

All simulations showed significant seasonal variability in the night time fraction of evaporation. In particular, it was predicted that the night time contribution increased considerably during the winter months, with all sites showing the fraction increasing to 55 -70%. This increase correlated well with an increase in the number of low wind hours and local instability over the water surface suggesting an increased frequency of free convective losses is responsible. Nonetheless, it is emphasised that despite the winter increase in the night time evaporation fraction, the overall magnitude and importance of the night time losses decreases from summer to winter, as does the day time component.

The similarity in the seasonal variability seen during this investigation is an interesting outcome since a common trend occurred regardless of the appreciable differences in meteorological forcing (particularly wind, humidity and air temperature) between the study regions. That is, the dynamical behavior predicted was largely insensitive to forcing meteorology, highlighting that water bodies are efficient self-regulators able to balance incoming solar radiation with outgoing latent heat (see Strub and Powell, 1987, for discussion of the feedback processes that regulate fluxes from surface waters).

Little variation was predicted for the different sized dams within a common climatic zone, emphasizing the one-dimensionality of the evaporation process. From a management perspective however, the importance of the evaporative loss relative to the overall water balance will vary as a result of different surface area to volume ratios.

# 4.2 Implications for reservoir design and management and evaporation amelioration

The study has highlighted several key design considerations. First, availability of necessary meteorological data is important for evaporation flux estimates. In this study, the focus was mainly on relative differences, but for actual design projects, access to accurate solar radiation and cloud cover (or long wave radiation) data will improve evaporation predictions. Second, the study has found that the night time fraction is mostly insensitive to climatic zone or dam morphometry, and should always be accounted for in water balance investigations and during the design of evaporation amelioration strategies. In particular evaporation estimation methods that solely rely on solar radiation, or use night time water level decline to calculate seepage will be erroneous. Finally, the results highlight that evaporation rates are not significantly impacted by storage configuration, although the overall volume lost through evaporation as a fraction of the total dam water balance can be minimized through careful storage design (i.e. minimizing the surface-area to volume ratio).

However, evaporation rates can be mediated through siting of the dam such that its exposure to winds from the dominant direction are minimized. It should also be noted that although a large fraction of evaporation occurs outside of sunlight hours, mitigation strategies that reduce solar radiation input would still be effective over the entire day since the surface water temperatures will be lower.

The present study has provided a simple and powerful tool for practitioners to conduct water balance investigations of irrigation farm dams. DYRESM is an efficient way to not only conduct water balance of a water body, but for a relatively small amount of input data, it is also able to accurately capture in detail the vertical thermal structure. As a result, surface water temperature predictions, which are important for evaporation calculation, are predicted to a high level of confidence when compared to other methods. Additionally, since DYRESM is based on a Lagrangian grid, it is particularly useful for long-term investigations that are typically of interest to natural resource managers and engineers.

Even without the added complexity of non-neutral stability corrections, still-air correction and wind-sheltering, DYRESM is able to provide useful estimates for design purposes as highlighted by the comparison in Section 3.3. For more detailed or specific studies of a particular site, then these complexities can be easily included for a more refined prediction.

Use of a common methodology between routine assessments is also advantageous as it encourages reproducible and consistent results. During this study, additions were made to improve the evaporation output to enable simple analysis of evaporation time series in third party programs such as Excel of Matlab. In particular, instantaneous, daily summations of evaporation, and the Monin-Obukhov stability parameter (z/L), have been incorporated into the model output file.

#### 5 REFERENCES

- Condie, S.A. and Webster, I.T. 1995, 'Evaporation mitigation from on-farm water storages. in reducing loss from evaporation': Report to the Cotton Research and Development Corporation, Sainty and Associates 1995, NSW.
- Condie, S.A. and Webster, I.T. 1997. The influence of wind-stress, temperature, and humidity gradients on evaporation from reservoirs. Water Resources Research, 33, 2813-2822.
- Hicks, B.B. 1975. A procedure for the formulation of bulk transfer coefficients over water. Boundary Layer Meteorology, 8:315-324.
- Hipsey, M.R. 2003. Improving rural dam efficiency in semi-arid Western Australia. MEngSc Thesis, University of Western Australia, Perth, Australia.
- Hipsey, M.R. and Sivapalan, M. 2003. Parameterizing the effect of a wind-shelter on evaporation from waterbodies. Water small Resources Research, 39(12): 1339. doi:10.1029/2002WR001784.
- Hipsey, M.R., Sivapalan, M. and Clement, T.P. 2004. A numerical and field investigation of surface heat fluxes from small wind-sheltered waterbodies in semi-arid Western Australia. Environmental Fluid Mechanics, 4: 79-106.
- Imberger, J. and Patterson, J. C. 1981. A dynamic reservoir simulation model DYRESM:5. In "Transport Models for Inland and Coastal Waters", pp310-361, H.B. Fischer (ed). Academic Press.
- Imberger, J., and J.C. Patterson. 1990. Physical Limnology, p. 303-475. In T. Wu [ed.], Advances in applied mechanics 27. Academic.
- Imboden, D.M., and A. Wüest. 1995. Mixing Mechanisms in Lakes, p. 83-138. In A. Lerman, D.M. Imboden and J.R. Gat [eds.], Physics and Chemistry of Lakes. Springer-Verlag.
- Launiainen, J. 1995. Derivation of the relationship between the Obukhov stability parameter and the bulk Richardson number for flux-profile studies. Bound. Layer Meteorol. 76: 165-179.
- Launiainen, J., and Cheng, B. 1998. Modelling of ice thermodynamics in natural water bodies. Cold Reg. Sci. Tech. 27: 153-178.
- Monin, A.S., and A.M. Obukhov. 1954. Basic laws of turbulent mixing in the atmosphere near the ground. Jr. Akad. Nauk SSSR Geofiz. Inst. 24: 163-187.
- Strub, P. T., and T. M. Powell. 1987. Surface temperature and transport in Lake Tahoe: inferences from satellite (AVHRR) imagery. Continental Shelf Res. 7: 1001-1013.
- Tennessee Valley Authority. 1972. Heat and mass transfer between a water surface and the atmosphere. Water Resources Research Laboratory Report 14, Report No. 0-6803.

- Watts, P.J. 2005. Scoping study Reduction of Evaporation from Farm Dams. Final report to the National Program for Sustainable Irrigation. Feedlot Services Australia Pty Ltd, Toowoomba.
- Webster, I.T., and Sherman, B.S. 1995. Evaporation from fetch limited water bodies. Irrig Sci 16: 53-64.
- Yeates, P.S. and J. Imberger. 2003. Pseudo two-dimensional simulations of internal and boundary fluxes in stratified lakes and reservoirs. Intl. J. River Basin Management, 1(4):279-319.
- Xenopoulos, M. A., and D. W. Schindler. 2001. The environmental control of near-surface thermoclines in boreal lakes. *Ecosystems*, 4:699-707.

